Quench Sensitivity of 6xxx Aluminum Alloys

by

Adam Assaad

A thesis

presented to the University of Waterloo

in fulfilment of the

thesis requirement for the degree of

Master of Applied Science

in

Mechanical Engineering

Waterloo, Ontario, Canada, 2016

Author's Declaration

I hereby declare that I am the sole author of this thesis. This is a true copy of the thesis, including any required final revisions, as accepted by my examiners.

I understand that my thesis may be made electronically available to the public.

Adam Assaad

Abstract

The use of AA6xxx series alloys continues to grow with the increasing demand for more fuel efficient vehicles. AA6xxx series alloys are commonly used in automotive applications because of their extrudability and good strength/weight ratio. As the use of these alloys becomes more prominent, new technologies must be developed to improve them. Chromium has been used as an alloy addition to AA6xxx alloys to control the grain structure by creating dispersoids that pin grains and limit grain growth and thereby improve the mechanical properties of aluminum alloys. However, the addition of chromium and other transition metals can have some adverse effects on aluminum alloys including making them more quench sensitivity after processing. The objective of this research was to do study the effect of alloy composition including the effect of Cr on the quench sensitivity of AA6xxx aluminum alloys, and to measure the effect of quench sensitivity on subsequent mechanical properties both in the T4 (naturally aged) and T6 (artificially aged) temper conditions. The experiments were conducted using a standard Jominy quenched end test and also included tensile testing for various quenching conditions for the AA6xxx alloys studied. The Jominy test provided a large range of cooling rates, which provided data for the variation in hardness as a function of cooling history. Supplemental tests were done on the alloys using tensile samples and water, air and furnace cooling to see what effect these cooling histories had on mechanical properties. It was found that the addition of Cr and Mn to the AA6xxx alloy caused an increase in quench sensitivity, and the cooling rate during quenching had a strong effect on the mechanical properties. It was found that AA6063 can be air cooled or cooled at a rate of ~0.8°C/s (48°C/s) after extrusion to retain 90% of its peak yield strength. Composition 1 (high Cr) must be cooled at a rate of at least ~25°C/s (1500 °C/min) in order to retain 90% of its

peak yield strength. Composition 3 (high Cr and Mg) must be cooled at a rate of ~30°C/s in order to retain 90% of its peak yield strength.

Acknowledgements

I would like to express my appreciation for my supervisor, Dr. Mary Wells, with whom I've had the pleasure of learning from for the past two years. Without her support and guidance, tireless efforts and strengths, the completion of this thesis would not have been possible. Thanks to Dr. Wells, I've learned more in these past two years of my life then I ever could have imagined.

I would also like to thank Dr. Massimo Di Ciano for all his help throughout the duration of this thesis. His help with the heat transfer model and laboratory techniques were extremely helpful.

I would like to thank GM Canada for their financial support, and for providing materials. Additionally, I would like to thank all the technical staff at the University of Waterloo: Mark Griffett, Yuquan Ding, and Nafiseh Moghimi for their help and efforts.

Lastly, I would like to thank my friends and family; without their support this journey would have been impossible.

Table of Contents

Table of Figures

1 Introduction

Interest in light-weighting vehicles and the use of AA6xxx series aluminum alloys in automotive applications has increased as the Corporate Average Fuel Economy (CAFÉ) regulations around the world have become more stringent. Referring to Figure 1-1, vehicle weight reduction represents the lowest cost near term solution to addressing CAFÉ and CO_2 reduction legislation. By switching to lower density aluminum extruded parts, the overall weight of vehicles is reduced, resulting in better performance of the vehicle and increased fuel efficiency.

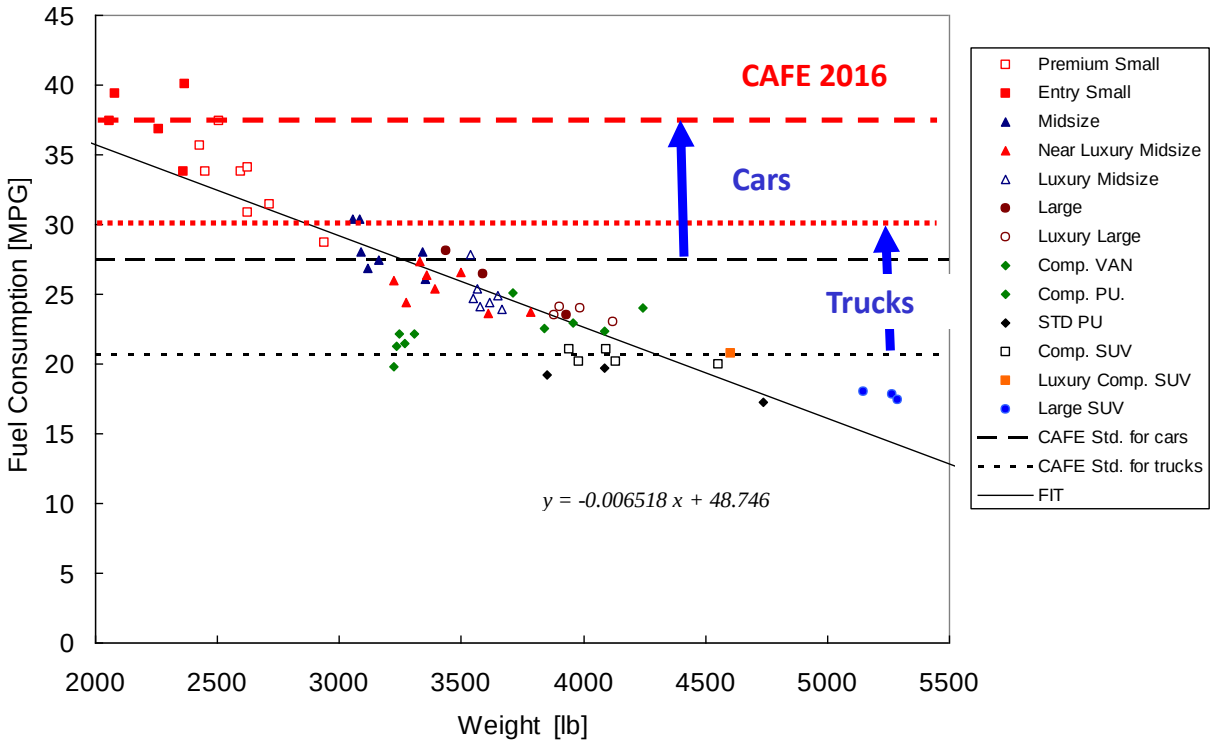

Figure 1-1: Relationship between car fuel consumption and car weight, showing CAFÉ standards for 2016 [1]

With the increasing demand for aluminum parts, the processes used to make parts must

be constantly researched and improved. AA6xxx aluminum alloys are considered viable candidates for use in automotive applications. These alloys are heat treatable medium strength alloys, commonly used for automotive parts because they not only have excellent strength to weight ratio, but also because, from a manufacturing perspective, they are very extrudable and can be made into complex cross sections. The aluminum extrusion process requires a billet to be pre-heated and then pushed through a die with the final desired cross-sectional geometry. The extrusion process results in large plastic deformation of the aluminum and changes to the microstructure due to the deformation. Typically, extrusion temperatures for the AA6xxx alloys exceed the solutionizing temperature such that all of the Mg_2Si which will later harden the material via an age hardening process dissolves into solution. Once the material has been forced through the die at the elevated temperature it comes out as an extrudate and depending on the alloy and final property requirements may be cooled either in still air, using fans or in some cases water quenched. Quenching can be done using a number of different media, in all cases the goal is to control the cooling rate of the material after the extrusion. Balanced against this is the need to minimize warping and high residual stresses of the final part which may occur if the cooling rates are too fast. The quenching process after extrusion can greatly affect the success of the heat treatment as too slow of a cooling rate will result in precipitation of the Mg_2Si along the grain boundaries and deteriorate the ability to strengthen the material during the subsequent age hardening treatment. Situations where heat treatable aluminum extrusions are age hardened directly after the extrusion process without using a separate solutionzing treatment are known as a T5 temper. The more common T6 temper is designated for cases when the aluminum is solutionized, quenched and then age hardened. Knowledge of the quench sensitivity of these alloys after the extrusion process is critical to understand what their subsequent response to the

age hardening heat treatment will be. Depending on the alloy chemistry certain aluminum alloys are not considered to be very quench sensitive, meaning that the amount of precipitation that occurs during quenching is not significantly affected by the quench rate, and slower quench rates can be tolerated and still allow the precipitates to remain within the solid solution. Other aluminum alloys may be extremely quench sensitive, meaning that variation in cooling rate may result in variation in mechanical properties. Quench sensitivity of an aluminum alloy depends both on alloy composition but also the thermal treatments such as homogenization experienced by the material as both of these parameters will dictate the dispersoid density in the alloy. Quench sensitivity data may be used to model what occurs after the extrusion, in terms of what cooling rate must be applied during the quench after the extrusion to achieve the necessary mechanical properties [3, 5-8].

AA6xxx series alloys are medium strength, heat treatable alloys whose main alloy additions are Mg and Si. These alloys are known for their excellent extrudability and machinability [2]. These alloys may be easily formed and then undergo a heat treatment to age the material and cause precipitates to form that significantly enhance the material strength. Processing of these alloys begins with Direct Chill (DC) casting into billets, followed by homogenization to remove any macrosegregation in the alloys. The homogenization treatment plays a role in quench sensitivity due to the formation of dispersoids that can then act as nucleation sites during subsequent quenching operations. Dispersoids are one of the precipitate phases formed during homogenization because the alloy is held at a high temperature for a long period of time. These dispersoids form due to free energy or thermodynamic requirements [9]. The distribution of precipitates and phases plays a large role in the aging kinetics and by extension mechanical

properties. In order to correctly study quench-sensitivity and the effect of alloy content on this, the same homogenization treatment must be applied to all the alloys studied.

Alloying elements such as chromium and manganese are often added to AA6xxx series aluminum alloys for a number of different reasons such as controlling grain recrystallization. Adding these elements may adversely affect the quench sensitivity.

As a result, a collaborative NSERC Automotive Partnership Canada (APC) research program was started between General Motors (GM), the University of Waterloo, McMaster University, the University of Sherbrooke, McGill University and CANMET Materials to develop AA6xxx extrusion alloys for an automotive front rail component.

2 Literature review

2.1 Al-Mg-Si System

The Al-Mg-Si or AA6xxx series aluminum alloys are a family of medium strength heat treatable alloys that rely on age hardening to produce their high strength via precipitation hardening. A significant advantage of the AA6xxx alloys is that they are also extrudable and are highly machineable making them a good choice for many applications [5-8]. The equilibrium phase diagram for this alloy system is relatively well known and referring to Figure 2-1, the system can be considered to be a pseudo-binary Al-Mg_2Si at a magnesium-to-silicon ratio of 1.73:1 (wt%) [10]. Referring to Figure 2-1, the pseudo-binary system has a eutectic at 595°C and ~15 wt% Mg_2Si. Excess silicon and magnesium reduce the solid solubility of Mg_2Si in aluminum, although the effect of magnesium is more predominant than that of silicon [10].

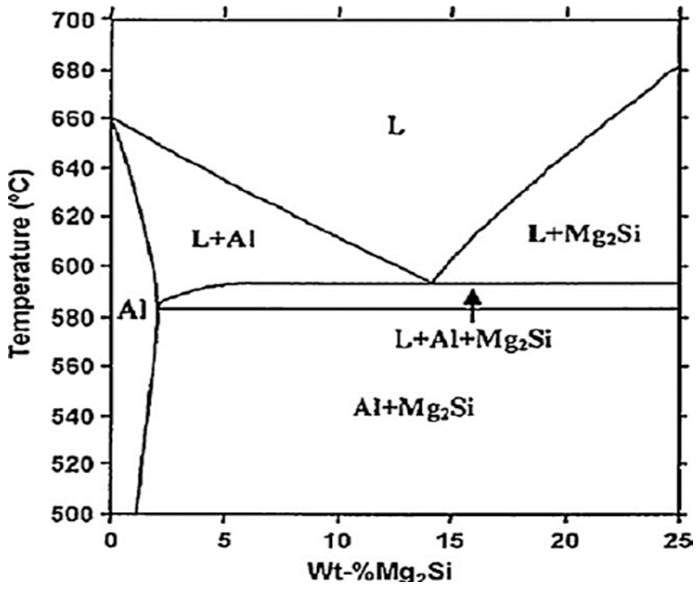

Figure 2-1: Pseudo-binary phase diagram for Al-Mg_2Si system [10]

These Al-Mg_2Si alloys can be divided into three categories. The first category includes alloys where the total amount of magnesium and silicon is less than 1.5%. A good example of this type of alloy is AA6063 which is mainly used in extruded architectural sections and contains

1.1% Mg_2Si [11]. Table 1 shows the range of nominal composition for a AA6063 aluminum alloy.

Table 2-1: Nominal composition AA6063 (wt%) [11]

Al	Cr	Cu	Fe	Mg	Mn	Si	Ti	Zn
≤97.5	≤0.1	≤0.1	≤0.35	0.45-0.9	≤0.1	0.2-0.6	≤0.1	≤0.1

With a solution treatment temperature of just above 500°C and low quench sensitivity, this alloy does not require separate solution treatment after extrusion; however, these alloys may be air quenched and artificially aged to obtain moderate strength, good ductility, and excellent corrosion resistance.

The second category of alloys contains 1.5% or more of magnesium and silicon. The addition of other elements, such as 0.3% Cu, increases the strength in a T6 temper condition. Manganese, chromium, and zirconium additions control the grain structure. Alloys such as 6061, which belong to this category generally, have a tensile strength of 310 MPa [11], whereas the previous category of alloys (6063) has a tensile strength of only 240 MPa in the T6 temper condition [11]. These alloys require a higher solutionizing temperature than the first category of alloys and are quench sensitive. Therefore, they require a solution treatment process followed by rapid quenching with a critical time of five seconds and artificial aging [16].

The third category of alloys contains almost the same amount of Mg_2Si, but they have excess silicon. In an alloy containing 0.8% Mg_2Si, the addition of 0.2% excess silicon increases the strength by 70 MPa [11]; without the addition, the tensile strength is only 230 MPa [11]. Nevertheless, large amounts of excess silicon are less beneficial. These alloys can experience grain boundary fracture in recrystallized structures due to segregation of excess silicon to the

grain boundaries. The effect of excess silicon can be counteracted by the addition of manganese, chromium, or zirconium, preventing recrystallization during heat treatment [10]. Common alloys of this group are Al 6351 and Al 6009.

In AA6xxx alloys, each alloying element has a specific purpose for it's addition. Chromium is added to control the grain structure and more specifically form many dispersoids to help prevent recrystallization and create a fibrous grain structure after hot deformation. Chromium will react with aluminum and silicon to form dispersoids which will start to precipitate out of the matrix during the homogenization heat treatment [5-8]. Manganese has very similar properties to chromium and is intended to also control recrystallization via the formation of dispersoids. Due to the large atomic size of Cr and Mn [5-8], these two elements are considered to be less mobile than elements such as Mg and Si [5-8] in the aluminum matrix. This slow diffusional effect leads to microsegregation in AA6xxx alloys. A suitable homogenization procedure must be selected to reduce microsegregation and uniformly distribute solutes through the solid solution. Dispersoids form when the solid solution is heated up to temperatures close to the solidus line. They typically form during homogenization and remain in the matrix during subsequent manufacturing operations. After manufacturing, the alloys can sometimes be age hardened directly (T5 temper) or solutionized and then age hardened (T6 temper). The faster the alloy is quenched after the manufacturing operation for a T5 temper or after the solution treatment for a T6 temper, the less likely Mg_2Si will precipitate during quenching. These Mg_2Si phases are hardening phases, to achieve maximum strength, these precipitates should be fully dissolved into solution, making them able to be precipitated during the aging treatment [4].

2.2 Effect of Thermal Cycle on AA6xxx Alloys

2.2.1 Homogenization and Solutionizing

Casting is followed by the homogenization heat treatment process. The overall aim is to remove the undesirable features of the as-cast microstructure and prepare it for extrusion. The aims of the homogenization process are:

- Dissolution of low melting eutectics
- Spherodisation of intermetallics
- Removing concentration gradients within grains
- Transformation of β-AlFeSi into α-AlFeSi
- Precipitation of secondary dispersoids

The process parameters, i.e. heating and cooling rate as well as homogenization time and temperature have to be chosen based on the metallurgical reactions listed above. Particular care has to be applied during cooling after homogenization as Mg-Si containing phases precipitate at temperatures below the Mg_2Si solvus. On the one hand, the cooling rate has to be high enough to avoid precipitation of coarse β-Mg_2Si in favour of finer, lath-shaped β'-Mg-Si-phases, which dissolve much more readily during billet pre-heating before extrusion [40]. On the other hand, if all Mg and Si are kept in solid solution, due to high cooling rates, flow stresses during extrusion are significantly increased.

Age hardening after extrusion is typically conducted in two steps: natural ageing, that occurs during room temperature storage and artificial ageing at elevated temperatures. In contrast to AA6xxx series alloys that are used in automotive body sheet applications and therefore experience natural ageing for several weeks, most extruded products are artificially aged within a few hours after extrusion. While natural ageing is known to have a negative effect at least on

alloys containing Mg+Si > 1wt.%, the process set up - artificial ageing is mostly conducted in batches of several extrusions - dictates natural ageing times between 30 min and 4 h. During the subsequent artificial aging process, the aim is to precipitate a high number of fine β-precipitates. Artificial ageing temperatures are chosen between 150 – 200°C. Higher temperatures result in a fast hardness increase but lower peak hardness compared to lower temperatures, which lead to higher peak hardness values after longer artificial ageing times. The optimal hardness occurs when the alloy is aged at 185°C for 5 hours.

Solutionizing is the process by which all the precipitates and other solutes in the solid solution are dissolved into solution by heating the alloy up to a temperature between the solvus and the solidus line of the desired phase [22]. In 6063 alloys, Mg_2Si is the phase that is desired to be dissolved into solution. As shown in Figure 2-2, the solution must be heated to 485°C in order to dissolve the Mg_2Si into the solid solution [13]. The goal of solutionizing is to dissolve the particles back into solution, in order to allow them to be precipitated during aging.

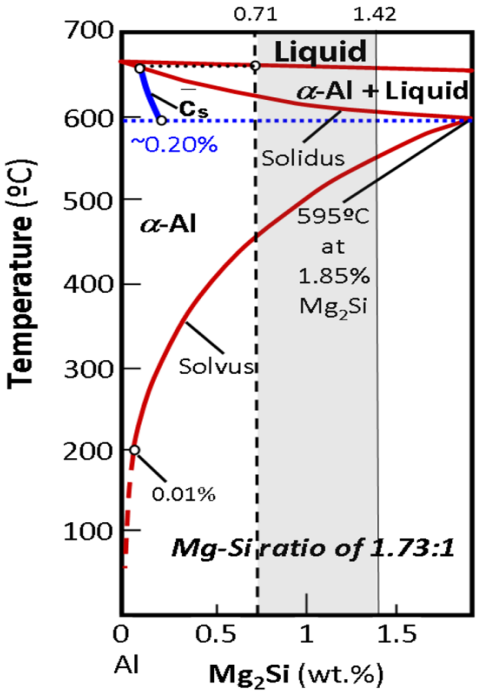

Figure 2-2: Pseudo binary phase diagram for AA6063 [13]

The equation for a regular solid solution, where B is soluble in A but A is virtually insoluble in B, is shown by equation 2.1 [12].

$$\mu_B^\alpha = G_B^\alpha + \Omega(1 - X_B)^2 + RTlnX_B \quad (2.1)$$

Where μ is the potential energy between two phases and **Ω** is the change in energy when one mole of A dissolves in B. This shows how temperature is related to the change in potential energy between phases. If the solubility of A in B is low, then equation 2.2 applies [12].

$$X_B^e = A\ exp\frac{-Q}{RT} \quad (2.2)$$

Equation 2.2 shows the effect of temperature on the solid solubility of B in A. This shows that by increasing the temperature, it is possible to dissolve B in A where it would otherwise be insoluble at room temperature [12].

Homogenizing is a form of solutionizing designed to help uniformly distribute precipitates that microsegregated during casting of the wrought alloy [9]. The amount of time necessary to homogenize until homogeneity is reached can be calculated. If it is assumed that C_B the concentration of solute B varies in a sinusoidal manner as a function of distance in one direction of the casting then eventually the sinusoidal function will decrease in amplitude until the concentration is approximately uniform in all directions [12].

$$C = \bar{C} + \beta_0\ sin\frac{\pi x}{l}, \quad \text{When t = 0} \quad (2.3)$$

In equation 2.3, $\bar{C}$ represents the mean composition, l is the distance in the x direction, and β_0 is the amplitude of the initial concentration profile. If it is assumed that the diffusion of B is independent of the concentration of the solution, then equation 2.4 can be rewritten as:

$$C = \bar{C} + \beta_0\ sin\left(\frac{\pi x}{l}\right)\exp\left(\frac{-t}{\tau}\right) \quad (2.4)$$

Equation 2.4 expresses the dependence of time on the relationship shown in equation 2.4 where time was assumed to be 0 [12]. The relaxation time is represented by the constant τ that accounts for the length of one cycle and the diffusion constant. If C at x =1/2 gives the amplitude of the concentration profile, then the following expression gives the amplitude [12].

$$\beta = \beta_0 exp\frac{-t}{\tau} \tag{2.5}$$

The homogenization time can be calculated by taking the limit as β approaches 0. If the amplitude is 0 then the line becomes flat and the concentration at any point of *x* becomes equal to the mean concentration [12]. Homogenization is important to quench sensitivity the dispersoids that form during homogenization will ultimately affect the quench sensitivity [9].

2.2.2 Quenching/Quench Sensitivity

Quenching is an important part of aluminum manufacturing. The cooling rate can play a major role in the overall mechanical properties of the alloy. This is mainly due to the fact that quenching is the precursor to the aging process, and the constituents in solution in the quenched state will affect the success of the subsequent aging operation [16-20]. After reaching the solutionizing temperature and holding at the desired amount of time, the precipitates are dissolved into the solid solution and no or very few precipitates should be left in the solid solution [14, 15].

Quench sensitivity is loosely defined as the dependence of material properties after age-hardening on quench rates after extrusion or solution treatment. It can affect mechanical properties such as strength, hardness and fracture toughness as well as the electro-chemical properties, corrosion and anodizing response. Quench sensitivity is attributed to attributed to precipitation of the strengthening phase forming elements during cooling at reduced rates and the

reduced concentration of mobile, non-equilibrium vacancies ("quenched-in vacancies") as a result of slow cooling.

Another way of looking at quench sensitivity is the ability of a AA6xxx material to tolerate slower cooling rates and not precipitate Mg_2Si out of solution when quenched slowly [4]. The importance of this appears during the aging procedure, if too much Mg_2Si precipitates out of solution, then there will not be enough Mg and Si left in solution to precipitate the desired β"-Mg_2Si out of solution [15]. The age hardening transformation sequence will be discussed in greater detail in section 2.2.3.

Keeping Mg and Si in solution is critical because when quenched slowly, only later forms of Mg_2Si such as β' will be present [15]. These are non-hardening phases and cannot be reversed back to β"-Mg_2Si unless the whole solutionizing process is redone. By elevating the temperature and allowing the required amount of time, the activation energy barrier is overcome and the precipitation sequence may continue, however if a transformation occurs where β-Mg_2Si (non-hardenable phase) has been formed during quenching, then this will result in a lowered amount of Mg and Si available for precipitation hardening [21]. Quenching too slowly can lead to reduction in vacancy supersaturation, unwanted precipitation, and over aging in certain parts of the alloy where precipitation has occurred [4]. This effect can be detrimental to the age hardening ability of the alloy.

Many who have previously studied quench sensitivity found that the addition of Mn/Cr increases quench sensitivity [5-8]. This happens because the addition of Mn/Cr increases the number of dispersoids that contain either of these two elements [5-8]. Mn/Cr dispersoids are good nucleation sites for β'-Mg_2Si particles during cooling [5-8]. Upon the addition of these two elements, quench sensitivity then becomes related to homogenization heating rate, temperature,

and time, as well as the cooling rate. By increasing the concentration of these two constituents, quench sensitivity will increase making it imperative that the alloys are quenched fast enough to avoid precipitation of Mg_2Si.

2.2.3 Aging

Precipitation hardening or age hardening is a process by which alloys that are age hardenable are elevated to a certain temperature that allows a series of transformations to occur resulting in the formation of precipitates [4, 23]. These precipitates cause lattice strain and increase the hardness of the alloy [15]. Precipitation occurs when the alloy is held at an elevated temperature much lower than the solutionizing temperature but high enough to overcome the energy barriers need for precipitation. The solutes dissolved into the supersaturated solid solution transform through a number of metastable states progressing from a less stable state to the most stable state which is known as the equilibrium phase. The following is a theoretical transformation where β' transforms into a more stable state [12].

$$\beta' \rightarrow \beta \tag{2.6}$$

By transforming into a more stable state, the system or solution is lowering the free energy and therefore wants to move towards this transformation. Diffusion must permit the above transformation to occur. By carefully controlling the temperature and time, two variables that can be manipulated, keeping the desired metastable state from transforming into a more stable state if it is undesired, is possible. Forming precipitates usually results in a decrease in free energy if creation of a nucleus will result in the destruction of a defect [12].

$$\Delta G_{het} = -V(\Delta G_v - \Delta G_s) + A\gamma - \Delta G_d \tag{2.7}$$

ΔG_d represents the free energy released by destroying a defect while $A\gamma$ refers to the interfacial energy term. The interfacial energy term is important because it will determine where nucleation

occurs, for example on a grain boundary or a free surface. The activation energy barrier that must be overcome is shown by the following expression [12].

$$\frac{\Delta G^*_{het}}{\Delta G^*_{hom}} = \frac{V^*_{het}}{V^*_{hom}} \tag{2.8}$$

This activation energy and the free energy shown in equation 2.8 is largely dependent on the interfacial energy term meaning that the type of nucleation site will play a large role in the likelihood of forming a precipitate. The thermodynamics of phase changes must be considered as it plays a large role in the formation of precipitates and predicting the outcome of aging procedures. Nucleation along grain boundaries and interphase boundaries such as a dispersoid, is more likely to occur at a faster rate than nucleation at vacancy sites or dislocations [4]. This is because ΔG_{het} is much lower for nucleation at interphase boundaries. The inclusion of dispersoids proves to be problematic to the aging procedure because Mn/Cr containing dispersoids prove to be favoured nucleation sites for unwanted β'precipitate nucleation [5-8]. The following is a schematic that represents the precipitation sequence in AA6xxx series alloys [4].

$$SS \rightarrow Mg/Si\ Co\text{-}clustering \rightarrow GP\ Zones \rightarrow \beta'' \rightarrow \beta' \rightarrow \beta\ (Mg_2Si) \tag{2.9}$$

In these alloys, β" is the hardening phase as due to the rod structure of the β" [24-29]. This stresses the importance of quenching because when the specimen is quenched fast enough there is enough Mg_2Si in solution that can transform into the various metastable transition phases [4, 24-29]. The formation of precipitates leads to an increase hardness from the extra stress needed to force dislocations through coherent zones [12]. The result of the formation of precipitates is an increase in misfit strain energy and an overall increase in mechanical properties such as hardness and yield stress. In order to be effective the aging sequence must be stopped at the β" and β' combination stage, or the precipitates become too large and dislocations are allowed to bow

through the strained zones, whereas β" hardening phases are shearable and are therefore more effective for hardening [4,12]. The growth of precipitates will happen naturally even after quenched by a process known as particle coarsening. This refers to the decrease in interfacial energy of larger particles and a desire to reduce the free energy of the system by the diffusion of small particles to larger ones. The transformation of transition phases stops when all the precipitates have reached their stable equilibrium phase β –Mg_2Si. The alloy at this point will be softer than at the peak-aged hardness. Aging for too long will result in an overaged alloy and a reduction in alloy strength [4,12].

2.3 Effect of Alloy Chemistry

2.3.1 Effect of Chromium and Manganese

For a long time, chromium has been used in combination with manganese to control grain structure. They typically have a limited effect on mechanical properties. Precipitates containing chromium are formed during homogenization; these precipitates are called dispersoids [5-8]. Due to high density and thermal stability, these dispersoids may act as nucleation sites for strengthening particles as well as affect recrystallization, grain growth, and recovery. α – Al(CrMnFe)Si is the phase present when both chromium and manganese are present [8]. When only chromium is present α-AlCrSi which is an FCC unit cell, as well as a phase known as α-Al(CrFe)Si [6]. These dispersoids all have complex structures which are incoherent with the Al matrix. Heterogeneous nucleation appears to be the suggested nucleation method of dispersoids [5, 30-31]. Various different nucleation sites have been suggested such as β" and β' needle structures [5]. To study the formation of dispersoids in AA6xxx series alloys containing Mn and Cr an electrical resistivity test along with TEM was conducted by Westengen et al. where alloys containing Mn were found to have a large variation in electrical resistivity during high

temperature annealing compared to alloys that only contained Cr [6]. This occurs because dispersoid formation is non-uniform and is subject to variation. Various researchers have noted that this can be controlled by slow heating [5]. Results from Logaard and Ryum's work shows that slow heating to roughly 250°C resulted in uniform distribution of dispersoids [5,6]. Electrical resistivity methods were used to find out the variation in precipitation by comparing an alloy with no dispersoid forming agents to an alloy with dispersoid forming agents [9]. According to this paper, it is believed that the addition of Mn/and Cr will affect the overall equilibrium solubility of strengthening particles containing Mg_2Si [5-8], this is however negligible because later results showed that the electrical resistivity between the two alloys were almost identical and the real difference occurs during the precipitation of Mn [5]. This study also showed that Cr precipitates more slowly than Mn, and precipitates at a higher temperature of roughly 490°C [5]. Logaard and Ryum's paper investigates a phase they call the U-phase" and in their paper it states that only this phase acts as a nucleation site for dispersoids not the β' precipitates [6].

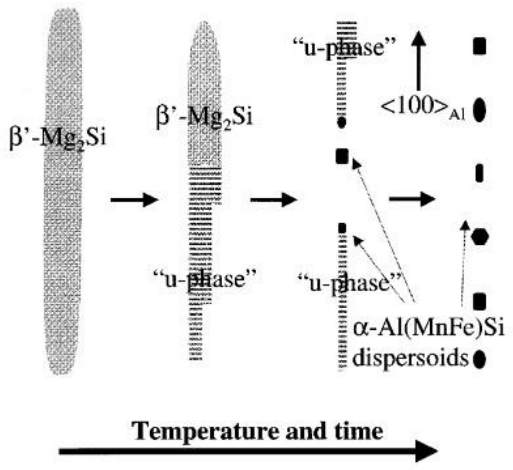

Figure 2-3: Schematic of Transformation from Precipitates to Dispersoids [6]

The nucleation method of dispersoids shown in Figure 2-3 occurs during homogenization and affects quench sensitivity by providing nucleation sites for hardening phase particles. Without the formation of these dispersoids, the alloy would be more tolerant to slower quench rates. Sheppard showed in his work that chromium can change fracture properties; the addition of chromium changes the failure mode from intergranular to transgranular [7].

2.3.2 Effect of Magnesium/Silicon on Mg_2Si

Mg and Si are two important elements found in AA6xxx series aluminum alloys. When they associate together they form the compound Mg_2Si. Stoichiometry dictates that there are 2 Mg atoms for every Si atom in this compound. Manufacturing an alloy and designing alloy chemistry requires the correct ratio of Mg to Si. The enrichment of certain phases or states with either Mg or Si must be considered in order to properly balance the alloy or even have an advantageous excess of one element. The equilibrium phase Mg_2Si or β-Mg_2Si is usually Mg enriched [9]. Metastable states such as β”-Mg_2Si are typically silicon enriched [9]. Having an excess of Si will result in the predominance of the metastable states given that the correct free energy requirements are met. Mg enrichment will promote the formation of the equilibrium phase.

Mg and Si also play a role in dispersoid distribution. Zhong et al. found that with decreasing Mg/Si ratio, there was a more homogenous distribution of dispersoids along with a higher dispersoid density [9]. This means that alloys containing Si enrichment promotes dispersoid formation. They also found that an excess of Mg slows down the natural aging process. It was found that Si enriched or alloys with a low Mg/Si ratio had an increased work hardening capacity [32]. The findings from this study show that there are many added benefits to increasing Si and increasing Mg, but too much of either could have negative effects. Figures 2-4

and 2-5 show the results from the Zhong et al. experiment, where Figure 2-4 shows a higher Mg/Si ratio and figure 2-5 shows a lower Mg/Si ratio [33].

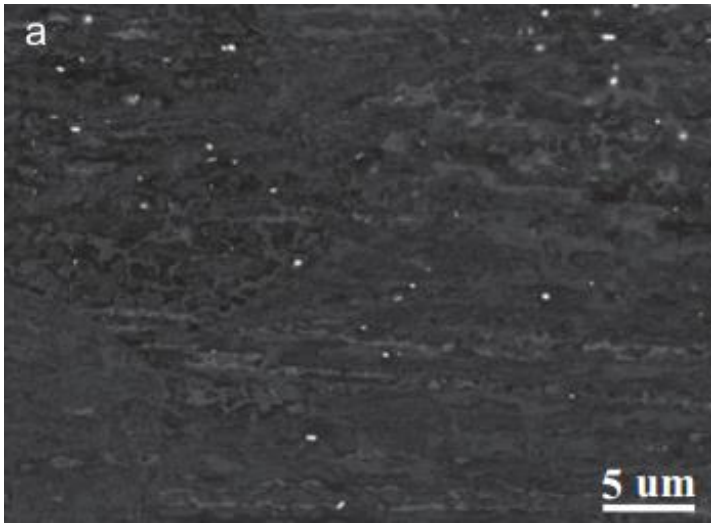

Figure 2-4: Dispersoid density of an alloy with a high Mg/Si ratio [33]

The white dots shown in the electron micrographs are the dispersoids. The grey contrasting in Figure 2-5 may appear due to some error in polishing with colloidal alumina suspension.

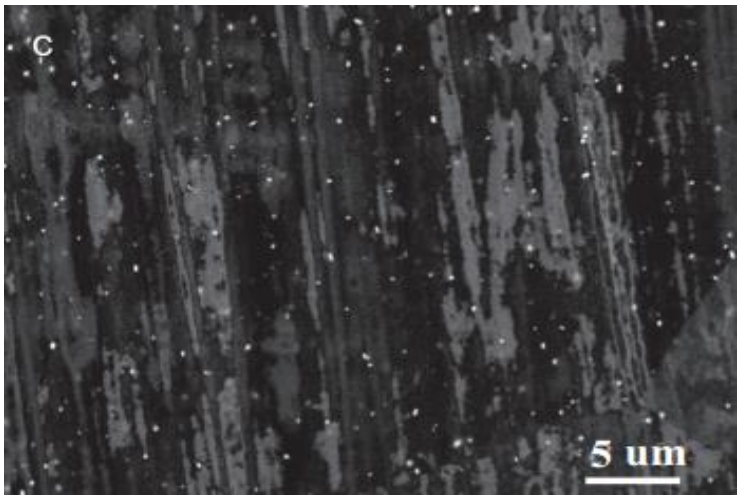

Figure 2-5: Dispersoid density of an alloy with a low Mg/Si ratio [33]

Zhong et al. found in their study that increasing silicon concentration within the matrix promotes the formation of dispersoids and increases dispersoid density as shown in Figure 2-5 [33].

2.4 Experimental Techniques for Studying Quench Sensitivity

2.4.1 Jominy Quench End Test

The Jominy end quench test is a test designed to measure quench sensitivity of an alloy. The test was originally designed to measure the hardenability of steel [34], however it was shown by other researchers that it could be an effect tool for other types of alloys including aluminum alloys. The test accomplishes this task by machining a Jominy bar out of the desired material and quenching the bar from one end giving a range of different cooling rates down the length of the bar. The hardness is then taken along the length of the bar in the axial direction and each hardness is corresponded to a cooling rate from each different section of the bar.

Newkirk and Mackenzie showed in their experiment that the Jominy test follows a one dimensional heat transfer model by measuring the hardness radially across the bar at a specific length. The results of their experiment are shown in Figure 2-6 [35].

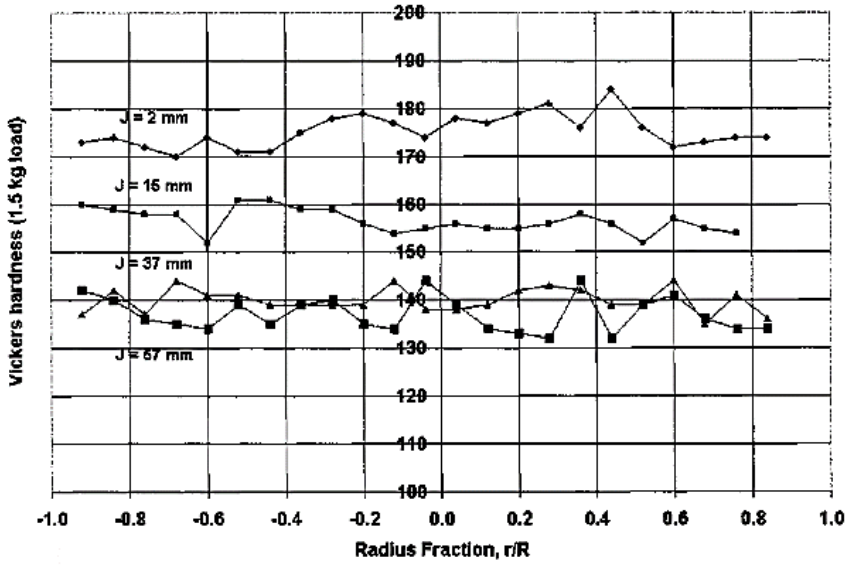

Figure 2-6:Vickers hardness across the radial surface of Jominy specimen showing 1D axial heat transfer [35]

The radial heat transfer according to the results of their experiment was shown to be negligible and it can be deduced that the heat is flowing through the bar axially [35]. Tanner and Robinson also did a study on the quench sensitivity of certain aluminum alloys using the Jominy method [20]. The results from their experiment are shown in Figure 2-7.

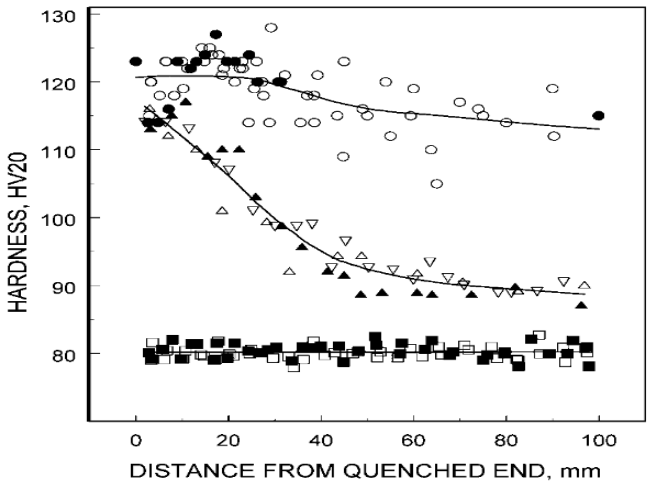

Figure 2-7: Hardness for Jominy specimens plotted against distance from quenched end, circles indicate 7010, triangles 7175 and squares 5083 [20]

Tanner and Robinson found that the quench sensitivity of some 7xxx series alloys is higher than 5xxx series alloys, showing that the Jominy end quench test can be used for aluminum alloys. The data collected from the Jominy bar may then be taken and related to the quench rate. Work previously done by Strobel et al. relate the hardness and quench rate to the dispersoid density and quench sensitivity [40].

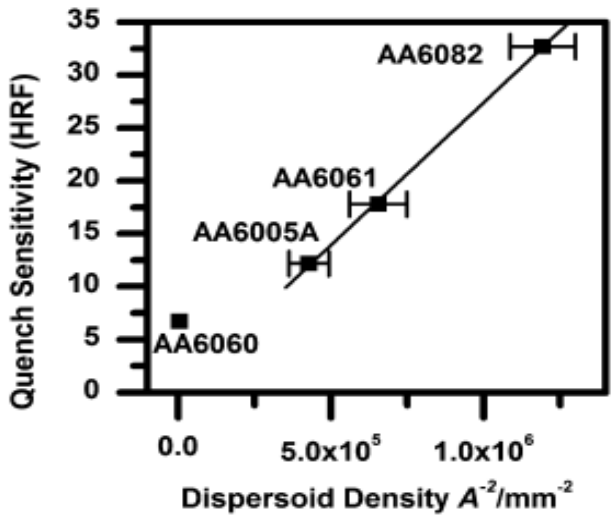

Figure 2-8: Relationship between dispersoid density and quench sensitivity [40]

3 Objective and Scope

With the increasing demand for low density alloys, aluminum parts are now more prominent than ever. As the use of aluminum increases, newer and better processes are being developed. AA6xxx aluminum alloys are frequently used in automotive production, and there is a greater desire now to improve these alloys than ever. Extrusion is among the most prominent forming techniques used for automotive applications. One potential way to improve aluminum alloys is through the addition of alloying elements. Chromium is commonly used in aluminum alloys to control grain growth and recrystallization. The addition of Cr may not always have advantageous effects; one of those disadvantages is that Cr is known to form dispersoids during homogenization, and Cr containing dispersoids may lead to an increase in quench sensitivity of the alloy. Quench sensitivity occurs when Mg_2Si in AA6xxx alloys, is allowed to precipitate out during the quenching procedure, as a result of inadequate quenching rates.

The extrusion of aluminum alloys may be done in such a way where during extrusion all of the Mg_2Si dissolves and no subsequent solution treatment is necessary, this is known as the T5 condition. This extrusion procedure is beneficial economically, and results in using less energy, as no separate solution treatment is required. If this process is to be implemented in alloys containing increased amounts of Cr, it becomes of interest to study the quench sensitivity of these AA6xxx alloys to understand the required quench rates after extrusion and the effect this will have on the final mechanical properties.

The objective of this research was to do an in depth study on the effect of Cr and other alloy additions on the quench sensitivity of AA6xxx aluminum alloys, and to see the effect of quench sensitivity on the mechanical properties of these AA6xxx alloys. This information will then be used to decide what type of quenching operation may be necessary after extrusion.

4 Experimental Methods and Materials

4.1 Materials

The AA6xxx alloys used in this experiment were industrially produced and supplied by GM Canada in the as-cast and homogenized state. The three different compositions used are shown in Table 2 and included: a baseline alloy (B), which was essentially a AA6063 alloy, composition one (C1) with a Cr and Mn addition for dispersoid formation, and composition three (C3) with increased Mg, Si, Cr, and Mn.

Table 4-1: Composition of AA6xxx alloys used in this research

AA6xxx	Si	Mg	Cu	Fe	Cr	Mn	Ti
AA 6063 (Baseline)	0.4	0.49	0.01	0.16	-	0.029	0.01
Composition 1 (C1)	0.4807	0.4965	0.148	0.195	0.182	0.0965	-
Composition 3 (C3)	0.5921	0.9171	0.1437	0.198	0.1974	0.0957	-

This research will help elucidate the effects of alloy composition of the AA6xxx aluminum alloys of their quench sensitivity after solutionizing. The supplied material was industrially homogenized using the following procedure: the material was heated to 560°C at a rate of 100°C/hour, the material was held at 560°C for 6 hours, and then the material was quenched with compressed air.

4.1.1 Alloy phase diagrams

Colleagues at McGill University in Professor Jung's lab who are partners in this research supplied thermodynamic database calculations for these alloys in the form of phase fraction versus temperature for each of the alloys being studied and shown in Figures 4-1 to 4-3.

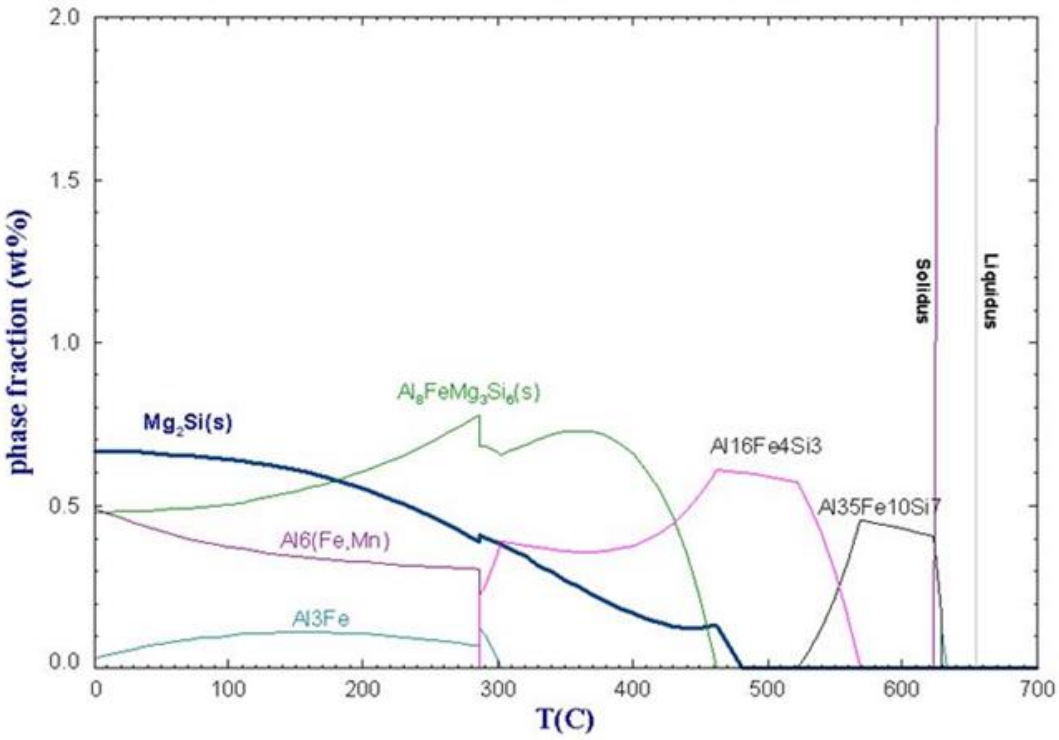

Figure 4-1: FACTSAGE predictions of phase fractions a function of temperature for the AA6063 baseline alloy.

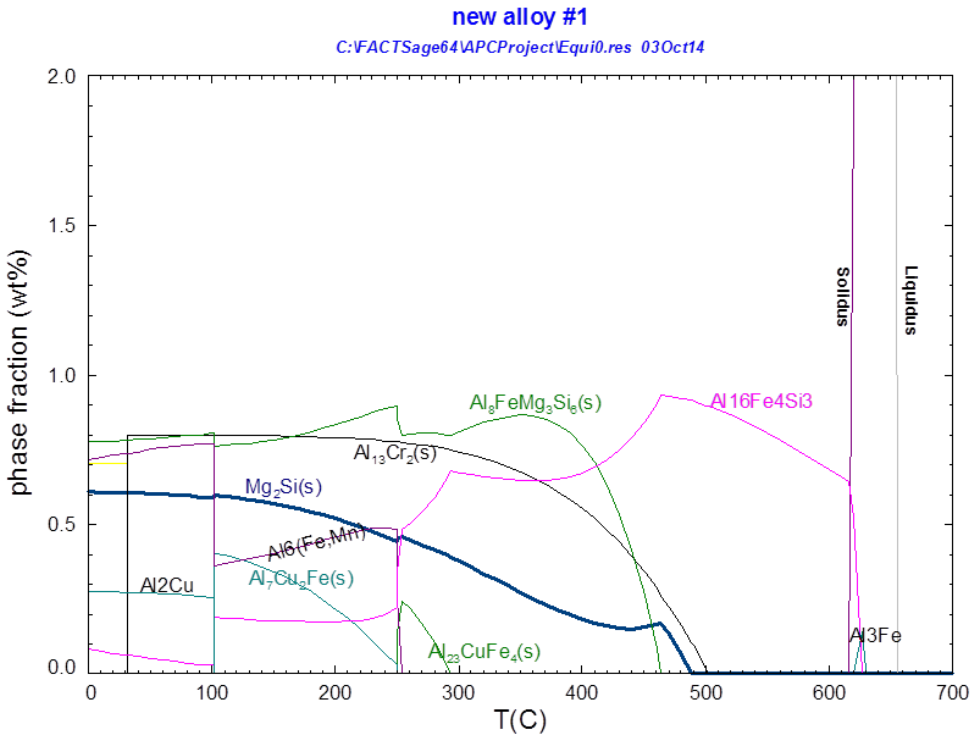

Figure 4-2: FACTSAGE predictions of phase fraction as a function of temperature for C1.

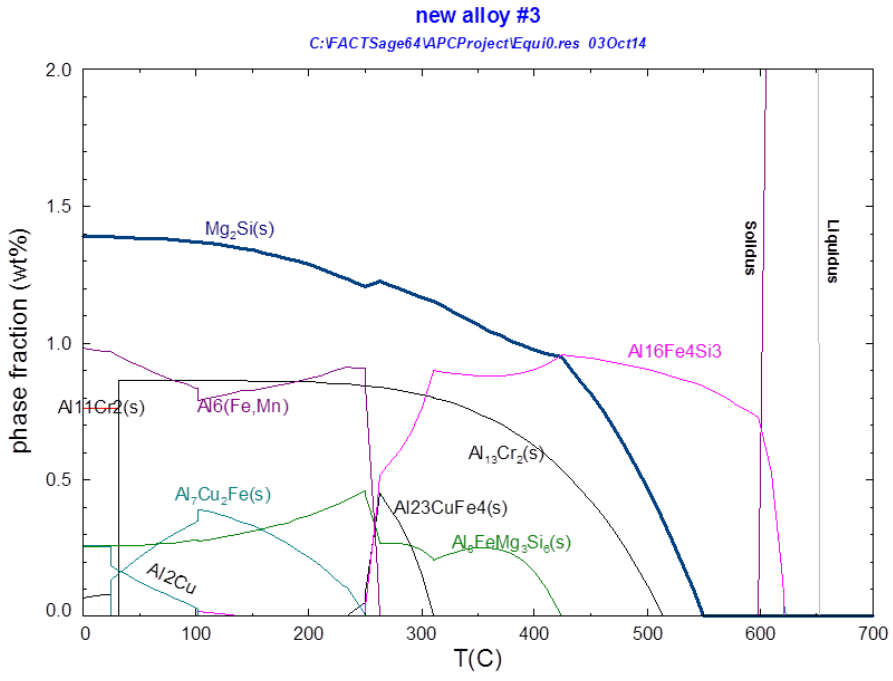

Figure 4-3: FACTSAGE predictions of phase fraction as a function of temperature for C3.

Table 4-2: Table summarizing data from FACTSAGE predictions

Alloy	**Solidus Temperature °C**	**Mg_2Si Dissolution Temperature °C**	**Equilibrium Mg_2Si at Room Temperature wt %**	**$Al_{13}Cr_2$ Intermetallics Predicted at room temperature**
Baseline	620	485	0.65	No
1	615	490	0.6	Yes
2	600	545	1.4	No
3	600	550	1.4	Yes

Table 4-2 shows the dissolution temperatures of the target precipitate Mg_2Si and the weight percent at room temperature. This also shows the difference between the predicted microstructural changes by adding different alloying elements in each alloy. The FACTSAGE predictions shown in Figures 4-1, 4-2, and 4-3 were used to help understand the range of phases present in the alloy under equilibrium conditions as well as predict the Mg_2Si dissolution temperatures, and will be explained in further detail in section 4.2.2.

4.2 Jominy Quenched End Test

4.2.1 Apparatus/Test Samples

A standard Jominy end-quench test was used to measure how quench sensitive each alloy was. This test was chosen due to its relative simplicity, it's availability at the University of Waterloo, ability to create a number of various cooling rates in a single sample, and because it worked within the material constraints. The Jominy test apparatus is known as a Jominy rig, containing an orifice that sprays water at the bottom of the bar, and a holder to hold the bar after it comes out of the furnace. Figure 4-4 shows a schematic for the Jominy rig set up, while Figure

4-5 shows the necessary dimensions and distance from the orifice as stated in the ASTM handbook, A255-10, pages 1-26.

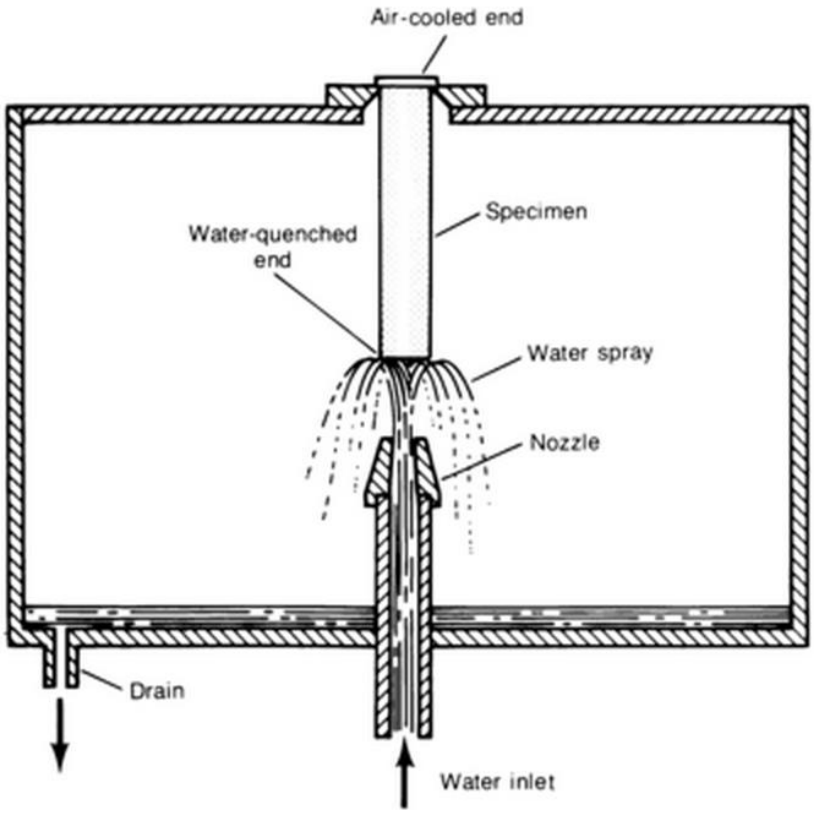

Figure 4-4: Schematic of a Jominy rig set up based on ASM handbook [38]

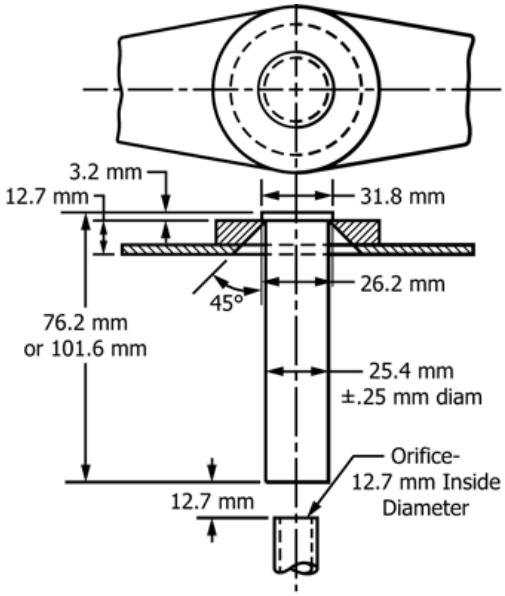

Figure 4-5: schematic indicating necessary dimensions for Jominy rig and test specimen from ASTM Handbook [34]

The most important dimension is that the orifice must be 12.7 mm. It is also imperative that water does not spill up the sides of test specimen to ensure the heat transfer remains one dimensional to the bottom of the specimen.

The test samples used in this study were modified slightly from the ASTM Jominy specifications. The ASTM specifications state that the bar should be 101.6 mm in length. Due to material constraints the length of the bars was shortened to 88 mm with a 12.7 mm cap was machined to give the full 101.6 mm of mass as shown in Figures 4-7 and 4-9. The bars also contained another modification: the bar was pre-milled to provide two flat surfaces. This is typically done after the quench is complete in a standard Jominy test; however, problems occur when the material is switched to aluminum. With steels, the local heating is not enough to affect precipitation, however based on the phase diagram of AA6xxx alloys, there was a risk of local heating affecting the precipitation in that region via age hardening and final hardness. It was for this reason that the bars were pre-milled.

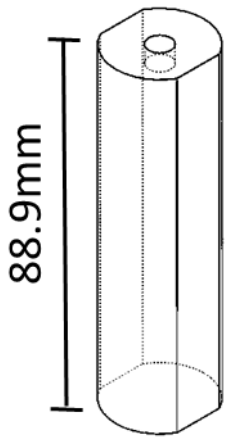

Figure 4-6: 3D Solidworks drawing of 88.9 mm bar used in Jominy test

A 3D solidworks model of the modified Jominy bars used in the experiments is shown in Figure 4-6. A screw to the cap shown in Figure 4-9 attaches this bar with the milled edges. Figure 4-7 shows the Solidworks drawing for the bar in figure 4-6.

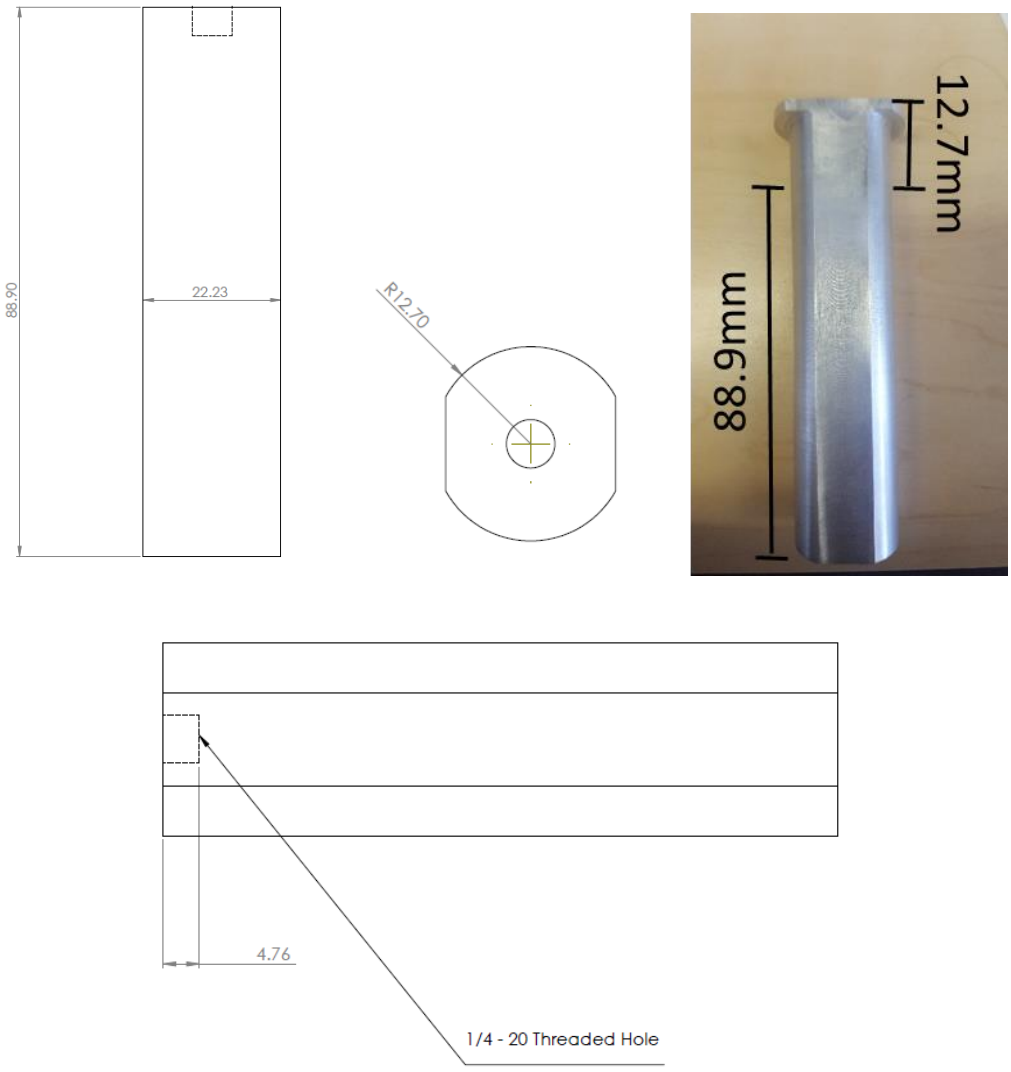

Figure 4-7: Solidworks drawing of 88.9 mm test specimen and an image of the specimen once cap is attached

Figure 4-7 shows the exact specifications for the test specimens. The material was taken from a homogenized DC cast billet. All specimens were taken from the billet at a distance of 25.4 mm to the center of the billet. The space was allotted all around the perimeter of the billet.

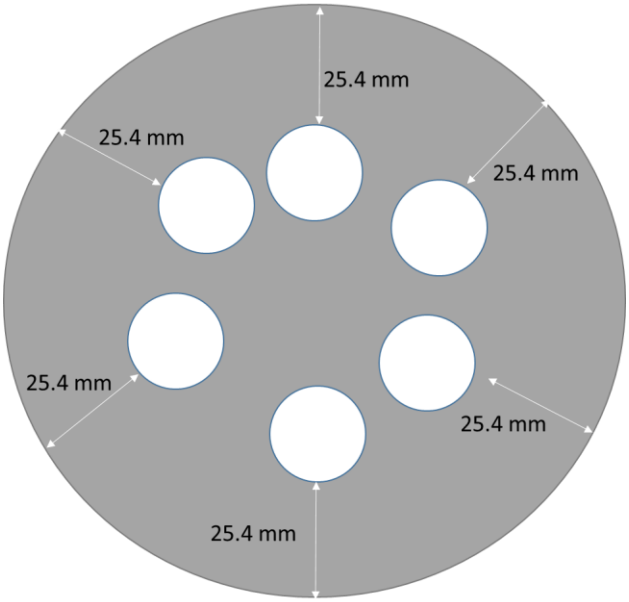

Figure 4-8: Cross section of homogenized DC cast billet showing locations where samples were extracted

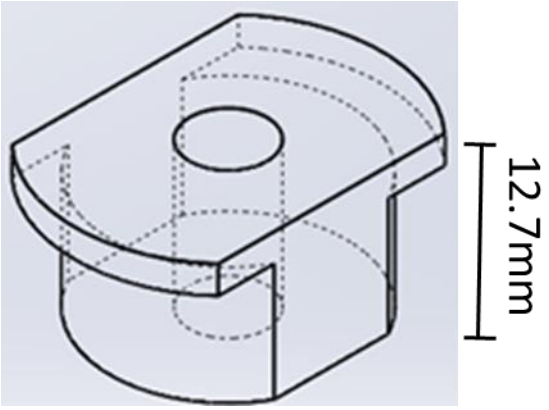

Figure 4-9: 3D Solidworks model of cap for 88.9mm bar

The cap shown in figure 4-9 is attached to the 88.9 mm bar using a screw going through the middle of the cap and down 4.76 mm into the bar. The purpose of the cap is to keep the heat transfer constant with the instrumented bars. The thermal conductivity of aluminum is high enough that the interface created between the cap and the bar provides negligible resistance to heat transfer. The top of the cap was extended by 7.6 mm in diameter to provide flaps that would hold the specimen up when placed in the holder of the Jominy rig. The caps were machined from samples taken from the same DC cast ingot as the 88.9 mm bars.

4.2.2 Procedure

The Jominy test involves 2-stages: the heating stage and cooling stage. The heating stage occurs when the specimen is placed into a furnace and allowed to reach the solutionizing temperature and is held there for a 10 minutes. The cooling stage is when the specimen is taken out of the furnace and is quickly placed into the holder of the Jominy apparatus, and is then quenched from the bottom end. Detailed information on the required time necessary to heat the specimen up to the solution treatment temperature was collected using thermocouple instrumented samples. This information is found in section 4.2.4.

The samples were prepared for solution treatment by attaching the cap to the 88.9 mm test specimen. After this step, the bar was then placed into a custom built dual-zone furnace and left to reach the solution treatment temperature of 560°C. The bar from the time it was put into the furnace until it was taken out was 67 minutes. 57 minutes were required to reach the desired temperature and 10 minutes were selected for the solutionizing time. Figures 4-1, 4-2, and 4-3 show FACTSAGE predictions of the various temperatures required for Mg_2Si dissolution. The Mg_2Si dissolution temperature for C3 is 550°C. To keep the experiment consistent, the same solutionizing temperature had to be chosen for all alloys. The lowest solidus temperature is found in C3, 600°C which is well above the Mg_2Si dissolution temperatures for all alloys. A solutionizing temperature of 560°C was chosen for all alloys. After completing the Jominy quench, the alloys were then all aged for 5 hours at 185°C, a standard practice to age 6063 alloys to the T6 condition [6]. The samples were left at room temperature for a week to naturally age, they were then tested in the T4 condition. The T6 samples were stored at -25°C and then aged within 3 days.

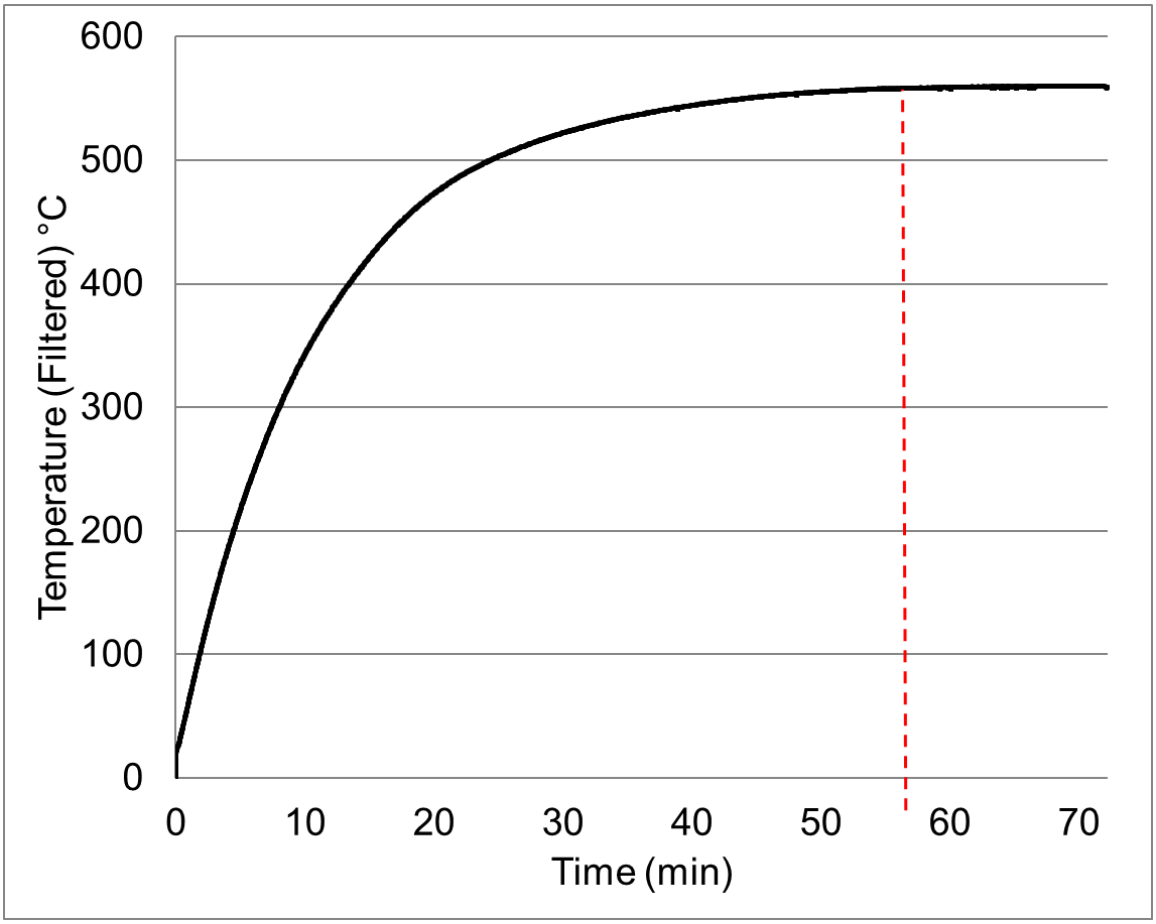

Figure 4-10: Heating data from instrumented Jominy bar with thermocouple at x = 40mm showing the necessary time required, indicated by the red dotted line, to heat the Jominy bar to 560°C

4.2.3 Hardness Profiles

Some of the Jominy specimens were left in the T4 for conditions (naturally aged for a week), while others were aged to T6. The hardness was taken in a line starting from the quenched end and finishing 40 mm from the quenched end of the bar. After 40 mm, the change in hardness measured was minimal. A different set of tests was designed to measure extreme cooling rates. A NANOVEA-M1 Nano indenter was used to make the indentations to measure the Vickers hardness. The standard metallurgical preparation procedure was used to prepare the sample. The 88.9 mm test specimen was cut at 42 mm from the quenched end. Then the sample was ground from 320 grit to 2400 grit using silicon carbide paper. Only one pre-milled side was

polished; the other side was ground to 600 grit to ensure the sample was sitting flat. The sample was then polished using STRUERS MD-Mol pads and 3 micron DP-Diamond Spray. MD-Nap pads were then used along with 1 micron DP-Diamond spray.

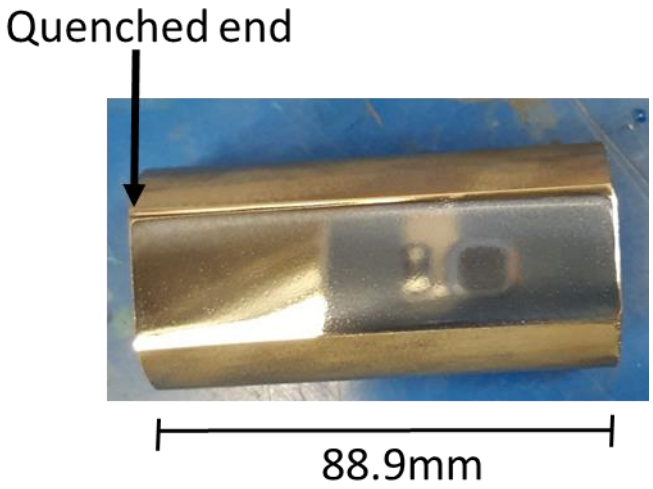

Figure 4-11: Jominy specimen after polishing

The sample was then placed in the NANOVEA and 40 indentations were made, starting at 0.2 mm from the quenched end. Each indentation was spaced 1 mm apart, going down the length of the specimen. The indentations were then observed under an OLYMPUS optical microscope. Lines were made along the two diagonals of the diamond indents; both diagonals were entered into the Vickers hardness formula shown in the following equation,

$$HV = \frac{2P\,sin(\frac{136}{2})}{d^2} = \frac{1.8544P}{d^2} \tag{4.1}$$

where P is the load in kgf and d is the length of the diagonal in microns. The hardness was then plotted against the distance from the quenched end, which is also known as a hardness profile.

4.2.4 Instrumented Samples and Calculating Cooling Rates

In order to obtain the cooling rates along different lengths of the bar, eight separate Jominy bars were instrumented with thermocouples varying in length. Figure 4-12 shows an example of a 3D Solidworks model of the Jominy bar with a 2 mm thermocouple depth. The 2 mm bar shows the thermocouple placed closest to the quench end, while the 60 mm bar shows the thermocouple placed furthest from the quench end. Thermocouples were placed at 2 mm, 4mm, 10 mm, 20 mm, 30 mm, 40mm, 50 mm, and 60 mm.

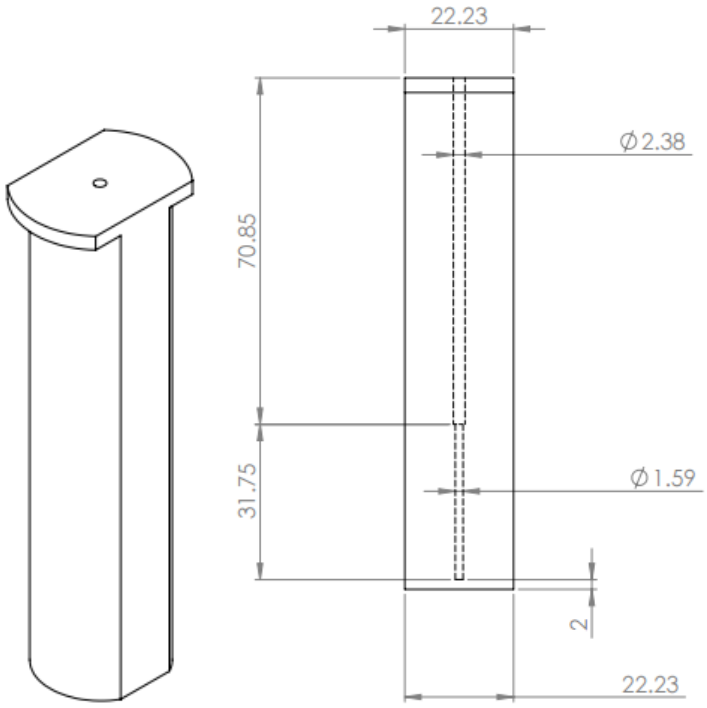

Figure 4-12: 3D Solidworks model along with specifications for instrumented Jominy bar with a thermocouple placed 2 mm from the quenched end

The data collected from the thermocouples was done using a NI USB-6212 data acquisition system. LABVIEW was the program used to acquire the data and apply the standard filter. After the heating and cooling data was collected, the filtered data was plotted as is to generate a time-temperature curve or cooling curve. The eight cooling curves were plotted on one graph to show the difference in cooling as the distance from the quench end increased.

The average cooling rate was then obtained by linearizing the cooling curves through averaging and removing noise from the data. The average of every 10 points was taken and plotted against the time at every tenth of a second. The first derivative was then taken and plotted against the time. Due to the nature of these alloys the important transformations occur during the cooling period from 500°C to 250°C during quenching. Based on this information, the average cooling rate was calculated between this temperature range.

To model the Jominy cooling process, a 1D transient heat transfer solution of a semi infinite solid is typically used. The assumption that the thermal diffusivity remains constant must be made in this scenario [39]. It must also be assumed that the bar is thermally insulated meaning that heat does not escape from the bar radially. With the case of surface convection, the following assumption must be made to create the boundary condition.

$$-k\frac{\partial T}{\partial x}\Big|_{x=0} = h[T_\infty - T(0,t)] \tag{4.2}$$

Where the thermal diffusivity remains constant and the surface of the solid is exposed to convection of a fluid with a constant temperature. In this case equation 4.3 shows the analytical solution to the PDE, complementary error functions must be used in the solution as there is no analytical solution to the integrals from this heat transfer equation [39].

$$\frac{T(x,t)-T_i}{T_\infty - T_i} = erfc\left(\frac{x}{2\sqrt{\alpha t}}\right) - \exp\left(\frac{hx}{k} + \frac{h^2\alpha t}{k^2}\right) erfc\left(\frac{x}{2\sqrt{\alpha t}} + \frac{h\sqrt{\alpha t}}{k}\right) \tag{4.3}$$

Table 4-3 contains the data used to solve the 1D transient heat transfer problem. The data from this table was entered into the solution to generate time-temperature curves showing temperature as a function of time for varying x values.

Table 4-3: Data and material properties used to solve 1D semi infinite transient heat transfer model

Symbol	**Property**	**Value**
Density	ρ	2635 kg/m^3
Thermal diffusivity	α	$\frac{k}{\rho Cp}$=0.000076 m^2/s
Thermal conductivity	k	212 W/mK
Heat capacity	C_p	1.06 J/Kg
Initial temperature	T_o	560°C
Water temperature	T_w	10°C
Heat transfer coefficient	h	29100 W/m^{2}K

4.3 Quench Sensitivity Tests/Extreme Cooling

4.3.1 Procedure/Test Samples

The Jominy bar gives a wide range of cooling rates, however it is of interest to investigate cooling rates even slower than the Jominy bar can offer. This is because the T4 condition commonly used in industry involves an air cooled environment. Automotive parts may sit in warehouses for up to 3 months before being used. These samples also provided the ability to test tensile samples for complete mechanical property determination. Three different quenches were performed creating three different conditions. A quench using water was designed to provide the fastest cooling rate. The second procedure was to leave the sample to air cool to simulate industrial conditions. The third procedure was to create an extreme condition, to achieve this the sample was heated to solution treatment temperature, the furnace was then turned off and left over night to cool.

To machine the samples a bar of each material with a radius of 12.7 mm was taken and cut with a lubricated vice saw to minimize any effects resulting from the heat cause by deformation of the material. Each sample was then cut to a length of 12.7 mm, creating a cylindrical sample. After the machining process, the sample was then placed into the dual-zone tube furnace and heated to the solutionizing temperature of 560°C. Based on data obtained from the instrumented samples, it was found that the sample took 27 minutes to reach the solutionizing temperature. The samples were left in the dual-zone furnace for 10 minutes solutionizing time, for a total of 37 minutes in the furnace for each sample. Figure 4-13 shows a schematic of the different heat treatments used to conduct these tests.

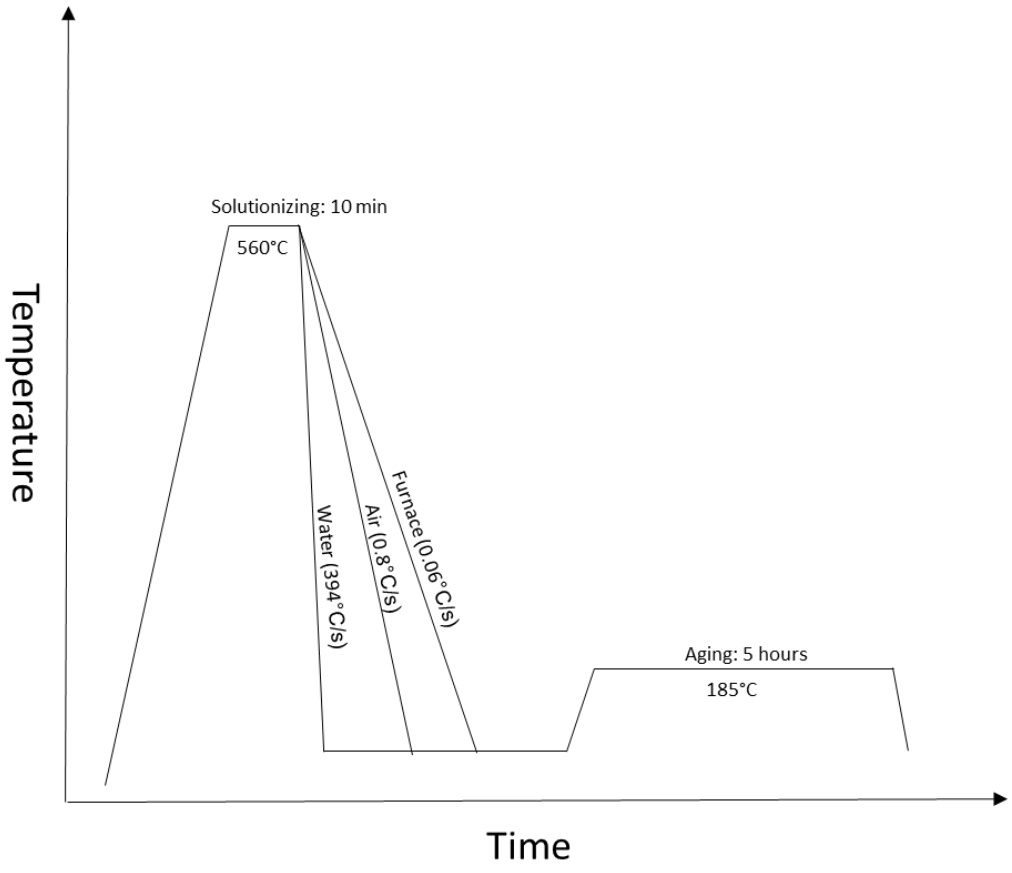

Figure 4-13: Schematic of heat treatments used in the procedure for extreme cooling rate tests

The samples were then aged for 5 hours at 185°C until they reached the T6 condition. The samples were then prepared via the standard metallurgical sample preparation method for Vickers hardness measurements.

4.3.2 Hardness Data

The NANOVEA-M1 Nano indenter was used to make the indentations to measure the Vickers hardness. In order to measure Vickers hardness, a flat and polished surface is required. The standard metallurgical preparation procedure was used to prepare the sample. The test specimen was ground using 180 grit paper to ensure both sides were of the specimen were flat. The sample was then ground from 320 grit to 2400 grit using silicon carbide paper. Only one side was polished; the other side was ground to 600 grit to ensure the sample was sitting flat. The sample was then polished using STRUERS MD-Mol pads and 3 micron DP-Diamond Spray. MD-Nap pads were then used along with 1 micron DP-Diamond spray. The sample was then placed in the NANOVEA and 5 indentations were made, starting from the left side and moving towards the right. Each indentation was spaced 5 mm apart, across the diameter of the specimen. The indentations were then observed under an OLYMPUS optical microscope. Lines were made along the 2 diagonals of the diamond indents; both diagonals were entered into the Vickers hardness formula shown in equation 4.1. The data was then averaged over all the points taken on each specimen. The new value was the average Vickers hardness for each different condition.

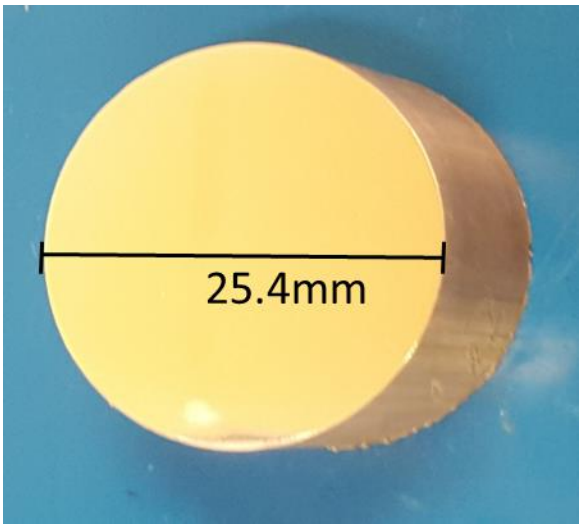

Figure 4-14: Example of sample used in one of the tests to show the effect of extreme cooling rates

4.3.3 Instrumentation and Cooling Curves and Calculating Rate

The cooling rates of each sample are important to calculate because there is a direct correlation between cooling rate and the mechanical properties after the T6 treatment. To do this for the 12.7 mm radius samples, the samples had to be instrumented with thermocouples. 1/16 inch holes were drilled from the side of the sample and move through the sample in the axial direction. The holes were drilled 12.7 mm deep. This was done to reflect the temperature at the middle of the sample, the last part of the sample to reach the equilibrium temperature. K^+ thermocouples from OMEGA were used to collect the data. The data collected from the thermocouples was done using a NI USB-6212 data acquisition system. LABVIEW was the program used to acquire the data and apply the standard filter. After the heating and cooling data was collected, the filtered data was plotted as is to generate a time-temperature curve or cooling curve. The average cooling rate was then obtained by linearizing the cooling curves through averaging and removing noise from the data. The average of every 10 points was taken and plotted against the time at every tenth of a second. The first derivative was then taken and plotted against the time. Due to the nature of these alloys the important transformations occur during the

cooling period from 500°C to 200°C during quenching. Based on this information the average cooling rate was calculated between this temperature range. The average cooling rate was calculated by averaging the first derivative between the temperatures of 500°C to 200°C. The data was then taken from these calculations and matched up with hardness values as well tensile tests.

4.4 Tensile Tests

4.4.1 Apparatus/samples

The tensile test was conducted using an INSTRON tensile tester. The tensile specimens were sub sized tensile specimens following the ASTM E8/E8M standards. Samples are typically made from sheet metal; however, the 6063 alloys were all in the billet form. The tensile samples were extracted from the billet and machined into the sub-size specimens. The samples had to be machined to a thickness of 6 mm to ensure the material did not bend upon removal from the billet. Figure 4-15 shows the ASTM E8/E8M standard for a sub-size tensile specimen.

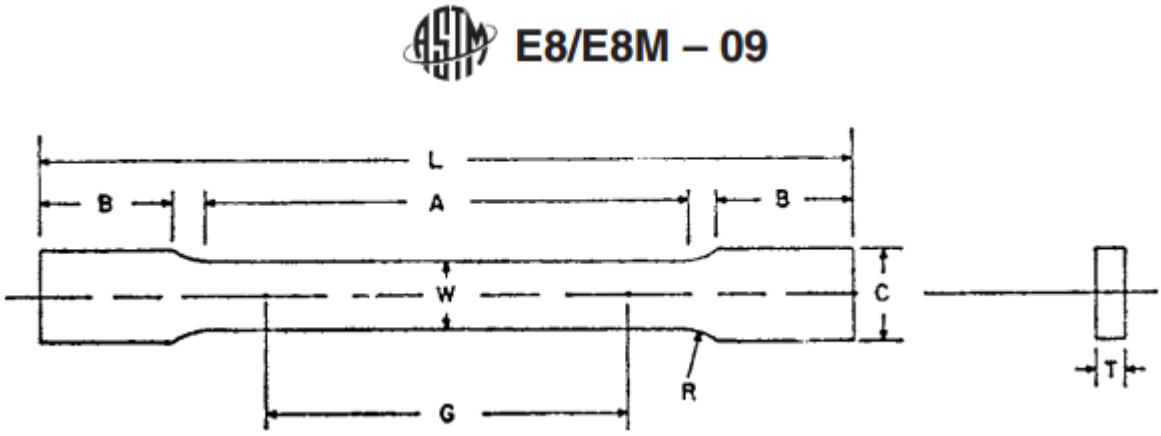

Figure 4-15: ASTM E8/E8M sub-size tensile standard used for tensile tests

The width of the gauge of the sample was 6 mm. The gauge length shown in Figure 4-15 by the letter “A” was 25.4 mm long. Each sample was prepared for tensile testing to a specified test condition corresponding to the extreme cooling rate tests found in section 4.3. A set of two

tensile specimens were prepared for each condition. For each alloy, three different conditions were applied to the tensile samples. The three conditions were: quenched in water, air-cooled, and furnace-cooled. After each quenching operation was complete, the samples were then aged to the T6 condition. The samples were aged in the custom built dual zone furnace at 185°C for 5 hours. The samples were quenched in water after the aging treatment to bring the sample back to room temperature.

Figure 4-16: Example of actual tensile sample used in this experiment

4.4.2 Procedure

The tensile test involves applying a load and measuring the corresponding displacement while applying the load. The load can be converted into engineering stress by using the following equation:

$$\sigma = \frac{P}{A} \tag{4.4}$$

Where P is the applied load, and A is the cross sectional area. The engineering strain can be calculated by using equation 4.5.

$$\varepsilon = \frac{\Delta L}{L_0} \tag{4.5}$$

The engineering strain is calculated by the elongation divided by the original gauge length of the specimen. Figure 4-17 shows the behaviour of mechanical plastic deformation on a material. During the tensile test, the specimen be pulled under axial tension and the specimen will continue to deform until fracture.

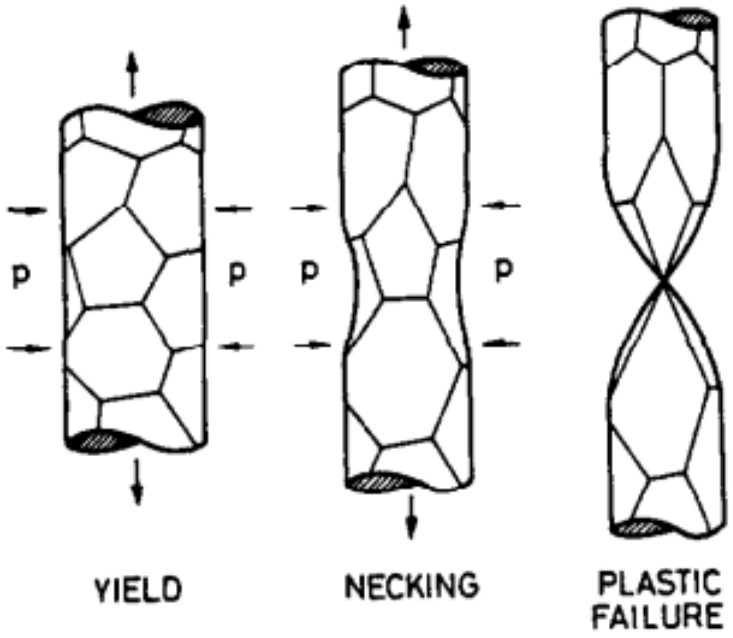

Figure 4-17: Schematic of plastic deformation behaviour of an alloy under axial tension [37]

Figure 4-17 shows a round test sample, the samples used in this experiment follow the specifications in Figure 4-16. The test specimens were loaded into the grips connected to the load cell by tightening the grips until the sample was tightly in place. The software provided by UNITED was then zeroed and the test was initiated. The strain rate was set to 1mm/min, with a data acquisition rate of 5 Hz. A 1-inch INSTRON extensometer modified for compatibility with the UNITED data acquisition system, was attached to the gauge of the sample. The test was run with the extensometer on till a strain of 1.5 mm. After this point the extensometer was removed and the test was allowed to continue. The displacement of the load cell was measured in millimeters after the 1.5 mm strain point. The specimen was pulled to strain failure and was then removed from the tensile testing machine. Table 4-4 shows the different conditions for each tensile test specimen and the number of times the test was repeated.

Table 4-4: Different alloy compositions and corresponding conditions, aging treatment, and repeat numbers for specimens used in tensile tests

Alloy Composition	**Condition**	**Aging treatment**	**Number of repeats**
Baseline	Water quenched	T6	2
Baseline	Air-cooled	T6	2
Baseline	Furnace-cooled	T6	2
C1	Water quenched	T6	2
C1	Air-cooled	T6	2
C1	Furnace-cooled	T6	2
C3	Water quenched	T6	2
C3	Air-cooled	T6	2
C3	Furnace-cooled	T6	2

Once the data was obtained it was processed by taking the average of the data from the two tests and using them to come up with the yield stress, UTS, and the elongation. The yield stress found by creating a 0.2% offset. This was done by fitting the straight part of the curve where the Young's modulus is found and creating a line. Then the equation of the line was found, and the line was shifted over by 0.2%. The stress at the point where the shifted line running parallel with the straight part of the curve and the stress-strain curve intersect is known as the yield stress. The UTS was determined graphically by finding the point that satisfies the following equation.

$$\frac{d\sigma}{d\varepsilon} = 0 \tag{4.6}$$

This point signifies a local maximum, and the stress at this point is known as the UTS. The two UTS values were averaged together to give an average UTS for each condition. To measure

elongation, two marks were placed at both ends of the gauge at exactly 1-apart prior to testing. After the test was concluded, the two marks were then measured using a caliper and the data was recorded. The data was then entered into equation 4.5 to give the percent elongation.

4.5 Metallography

4.5.1 Sample Preparation

Samples of interest were prepared using the metallographic sample preparation procedure. Four of the samples from section 4.3 used in the extreme cooling rate measurements were prepared for examination. Any rough edges on both sides of the sample were removed by using 180 grit silicon carbide paper. The edge not being examined was then polished using 320 and 600 grit silicon carbide papers till a flat surface was achieved. The samples were large enough that no metallurgical mounting procedure was required. The side to be examined under the SEM was also polished using 320 and 600 grit silicon carbide paper. After this step, 1200 grit and 2400 grit silicon carbide paper were used. Samples were ground for roughly 5 minutes for each grit using a STRUERS Roto-Pol 31. After this step, the sample was polished using STRUERS MD-Mol pads and 3 micron DP-Diamond Spray. MD-Nap pads were then used along with 1 micron DP-Diamond spray. MD-Nap along with ¼ micron DP-Diamond Spray from STRUERS were then used in the final polishing step. The samples were then correctly stored until the examination time, where the etchant procedure was conducted approximately one hour prior to SEM examination.

4.5.2 Etching Procedure

The 4 samples were etched approximately one hour prior to examination. 75 mL of etchant was prepared by adding 25 mL of hydrochloric acid, and 25 mL of nitric acid to 25 mL of methanol. 1 drop using an eye dropper of hydrofluoric acid was then added to the solution to

prepare the etchant. A petri dish was then filled with the etchant and the areas undesired for etching were covered using platers tape. The sample was then immersed into the etchant and the sample was held there for 30 seconds. After the sample was then rinsed using water and methanol and quickly air dried. The sample was then cleaned using the ultrasonic cleaner for 3 minutes per sample. The samples were then quickly dried again using compressed air and the sample was taken for SEM examination.

4.5.3 SEM Procedure

The SEM used to characterize the microstructure was a ZEISS 1530 FESEM, a state of the art piece of equipment. The SEM was able to resolve structures as small as 2 nm. The four selected samples; baseline water quenched, baseline furnace cooled, C3 water quenched, and C3 furnace cooled were all in the as quenched condition and unaged. The samples were then placed into the sample holder and placed in the vacuum chamber. To view the samples, the correct field must be selected in the SmartSEM software used to navigate the SEM. Baseline furnace cooled was conducted on its own in field 1. Once the samples were inserted onto the stage found in the vacuum chamber, the gate was shut and the vacuum process was initiated. An accelerating voltage of 15 kV and 5 kV were both used to image the specimens. Images were taken in both secondary electron mode and AsB backscatter mode.

5 Results and Discussion

5.1 Jominy Quenched End Test Cooling Rates

The hardness profiles were an effective way to study the change in mechanical properties along the length of the Jominy bar based on difference in cooling rates. It was of interest to know the cooling rates that corresponded to the changing distance from the quench end of the Jominy so that hardness measurements could be correlated to cooling history.

5.1.1 Measured Cooling Histories

As described in the methodology section, the Jominy bars were instrumented with type K thermocouples so that detailed knowledge of the thermal history experienced during cooling could be obtained. Figure 5-1 shows typical measured cooling rates for different positions along the Jominy bar during cooling of AA6063. For visual clarity the start time of each location was offset by 10 seconds.

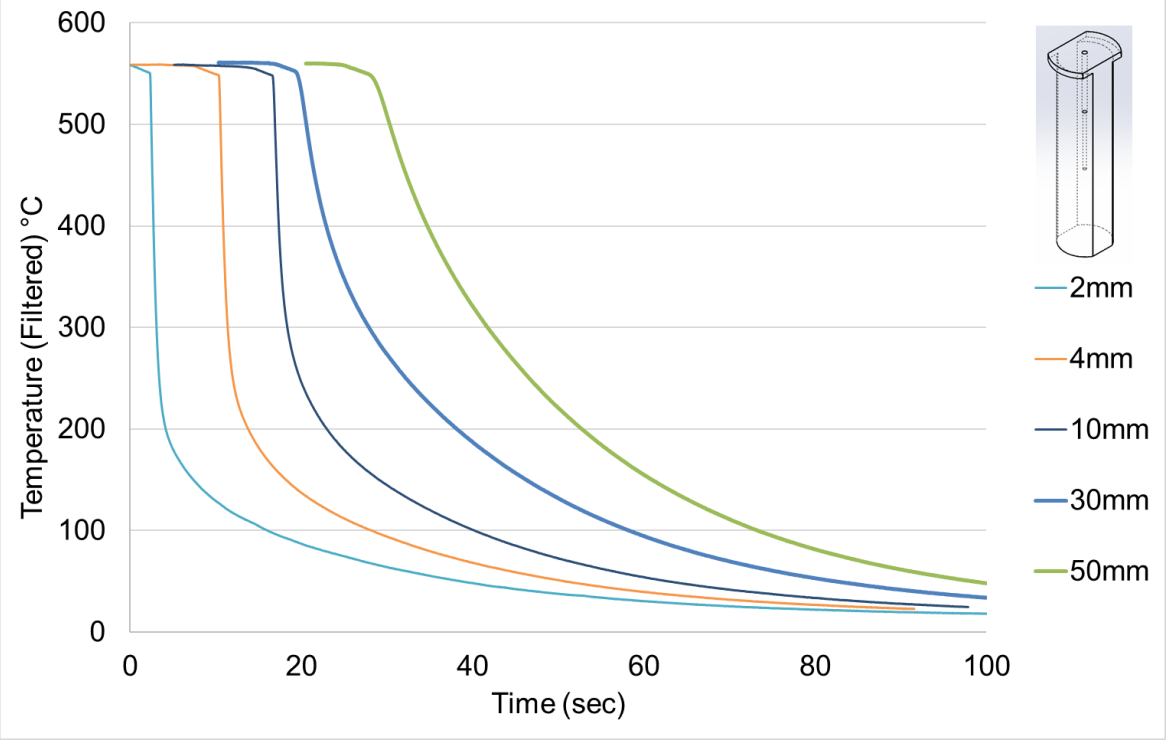

Figure 5-1: Measured cooling histories from the quenched end of the Jominy bar during cooling of AA6063

To determine the average cooling rate during cooling, cooling histories between 500°C and 250°C were considered at each location, as this is the critical temperature range over which precipitation of the Mg_2Si will occur [19]. Figure 5-2 shows an example of how the average cooling rate was calculated for each location.

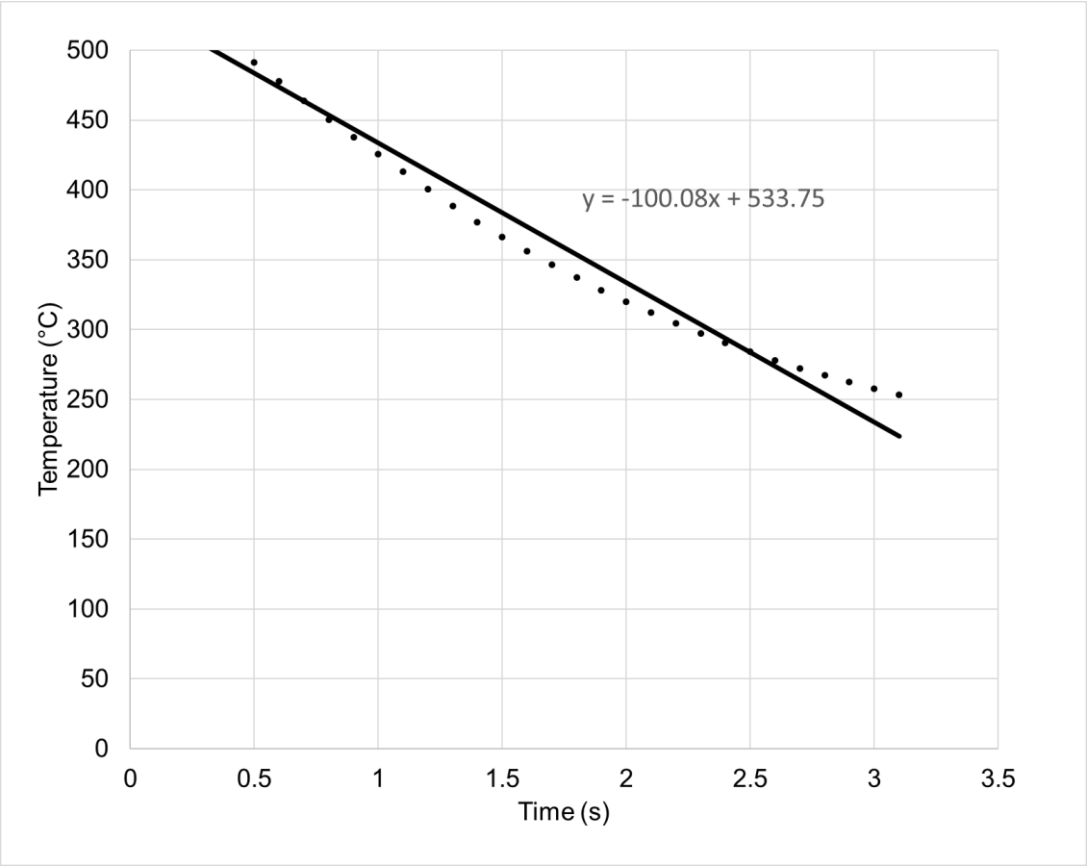

Figure 5-2: Calculation of average cooling rate along the Jominy bar

5.1.2 Analytical Solution of Jominy Cooling Curves

Previous research [41] had shown how the Jominy quench test could be approximated as a 1D transient heat condition heat transfer problem and solved analytically. In this research, a similar approach was used and the a 1D transient heat transfer of a semi-infinite solid model was solved to predict the cooling history at different positions along the Jominy bar as a function of distance from the quenched end.

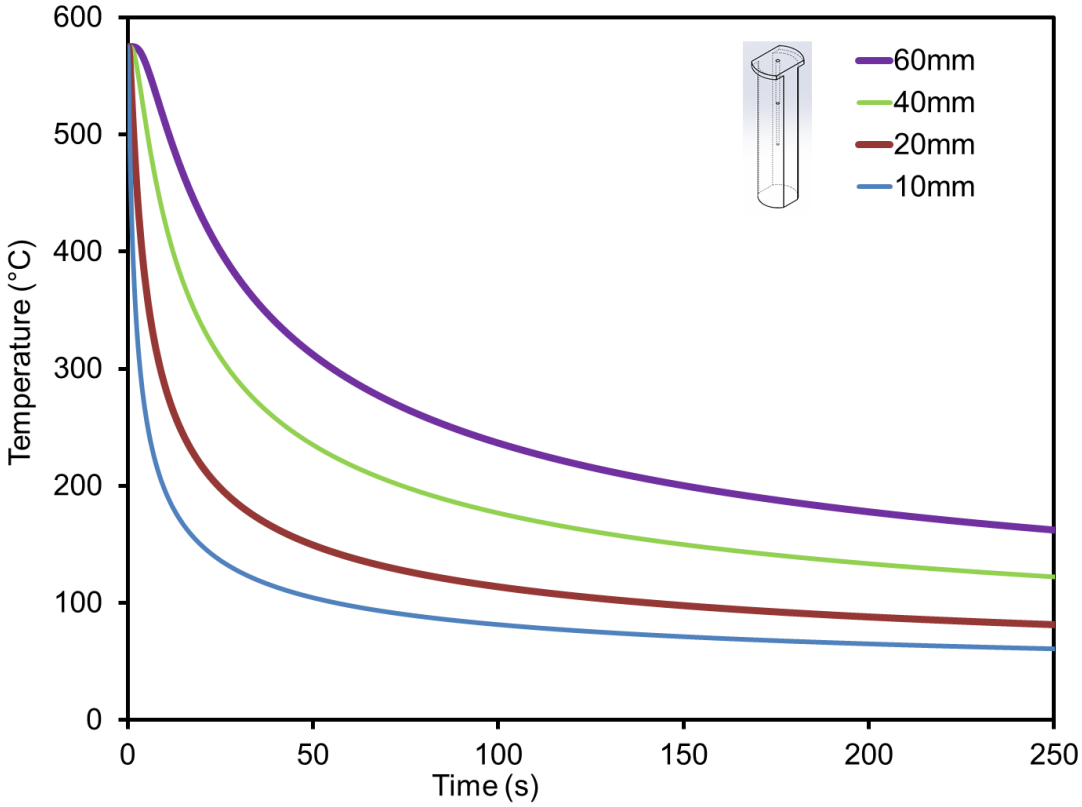

Figure 5-3: 1D transient heat transfer solution of a semi-infinite solid where T_0= 560°C and T_w = 10°C, h= 29100 W/m^{2}K

Figure 5-3 shows the 1D transient heat transfer model predictions for a semi-infinite solid that was conducted to simulate the cooling of a Jominy bar from 560°C to room temperature. The analytical solution was solved using equation 4.3 and the boundary conditions shown in equation 4.2. To come up with the solution, the heat transfer coefficient at the end was altered until the fit between the measured data at that location and predicted thermal history based on the 1D transient heat transfer solution close to the end at the 2 mm position fit well. Further from the quenched end the measured results deviated from the model predictions and indicated that perhaps heat loss to air during cooling of the bar started to play a role and the assumption of 1D heat transfer became less certain.

The measured temperature-time data shown in Figure 5-1 was plotted in such a way that all the lines were shifted away from each other by *x=10s* in order to give a better visual clarity of the cooling curves at the different locations.

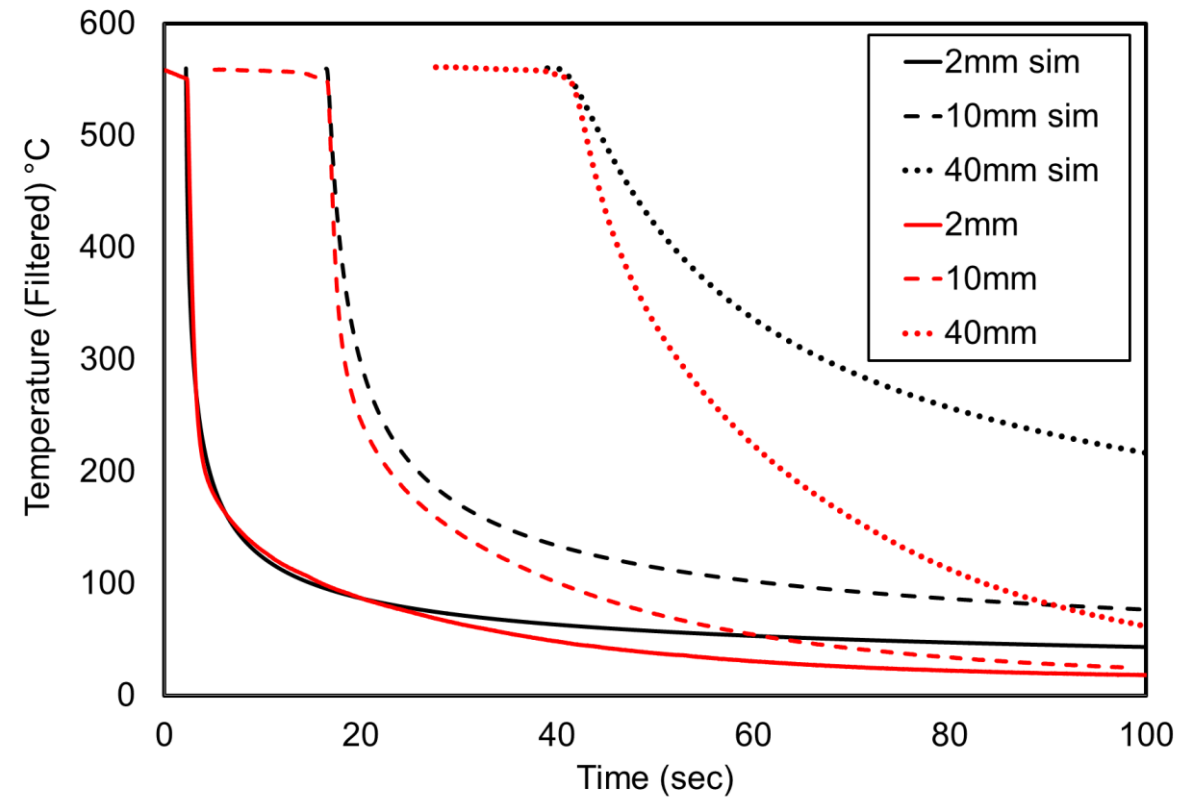

Figure 5-4: Comparison between calculated cooling curves (black) and measured cooling curves (red)

The experimentally obtained results show reasonable agreement with the calculated cooling rates close to the quenched end however at locations further from the quenched end (i.e. 40 mm) the measured and calculated results start to deviate substantially. This is likely due to the fact that the Jominy bar is not thermally insulated and the model assumes that heat is only lost in one direction. In reality, some heat is lost from the radial surface of the Jominy bar causing the bar to cool slightly faster than predicted. The boundary conditions assumed in the model were calculated using data found by Wells et al. [42] and the heat transfer coefficient was averaged

over the entire cooling process which again is an oversimplification to a more complicated boiling heat transfer problem.

5.1.3 Average Cooling Rate

To combine the results from the Jominy test, and the average cooling rate (between 500°C and 250°C) corresponding to the distance from the quenched end was calculated and plotted against the distance from the quenched end. Figure 31 shows the results of the calculated average cooling rates from the thermocouple data, versus the distance from the quenched end.

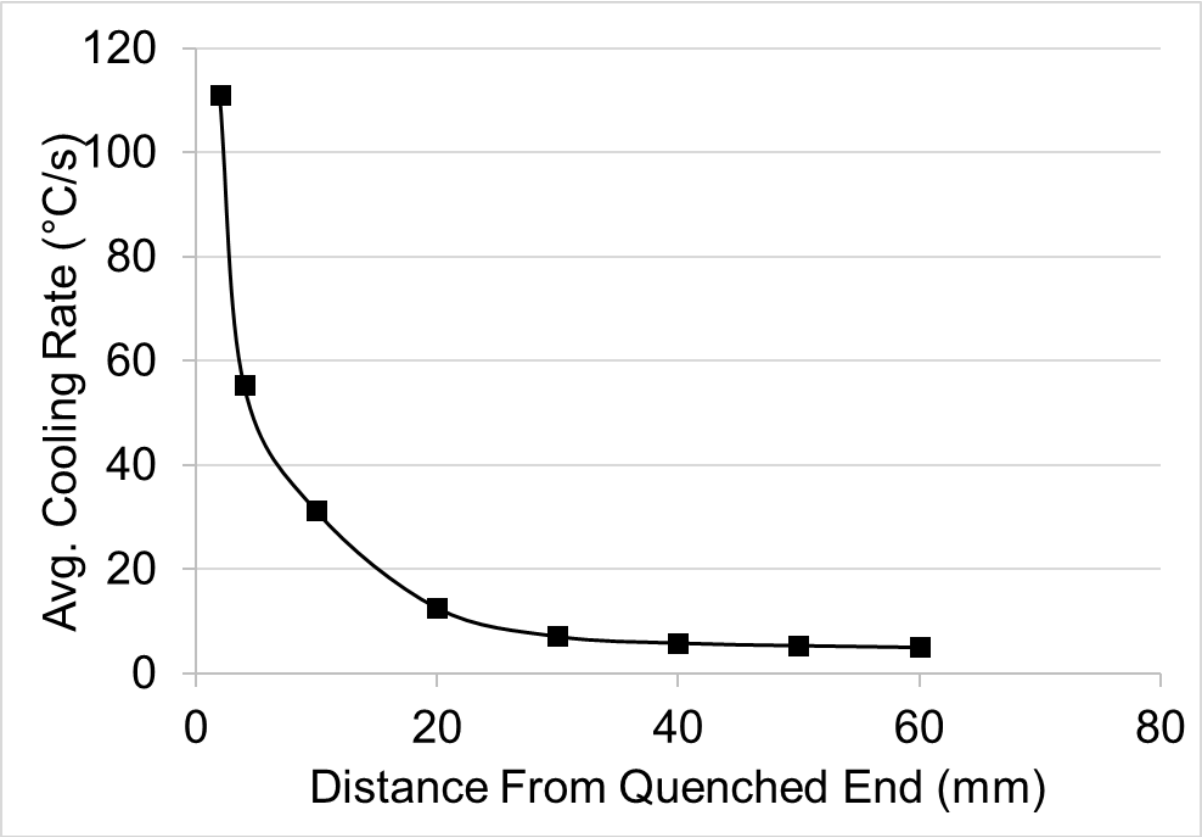

Figure 5-5: Average cooling rate versus distance from the quenched end, each cooling rate is an average of the cooling rate at the corresponding distance from the quenched end, in reality the cooling rate is not linear but varies as a function of time and distance

Using this graph, the cooling rate at any position along the Jominy bar can be obtained and a measured hardness can be correlated to a cooling rate. As shown in Figure 5-5, the cooling rates are highest close to the quenched end and rapidly decrease along the length of the bar.

5.2 Other Cooling Tests

5.2.1 Cooling Curves

To measure the cooling rate for each condition for the other cooling rate tests, cooling curves were constructed by instrumenting the samples with thermocouples. The results for the measured cooling curve of the water, air and furnace quenched samples are shown in Figure 5-6.

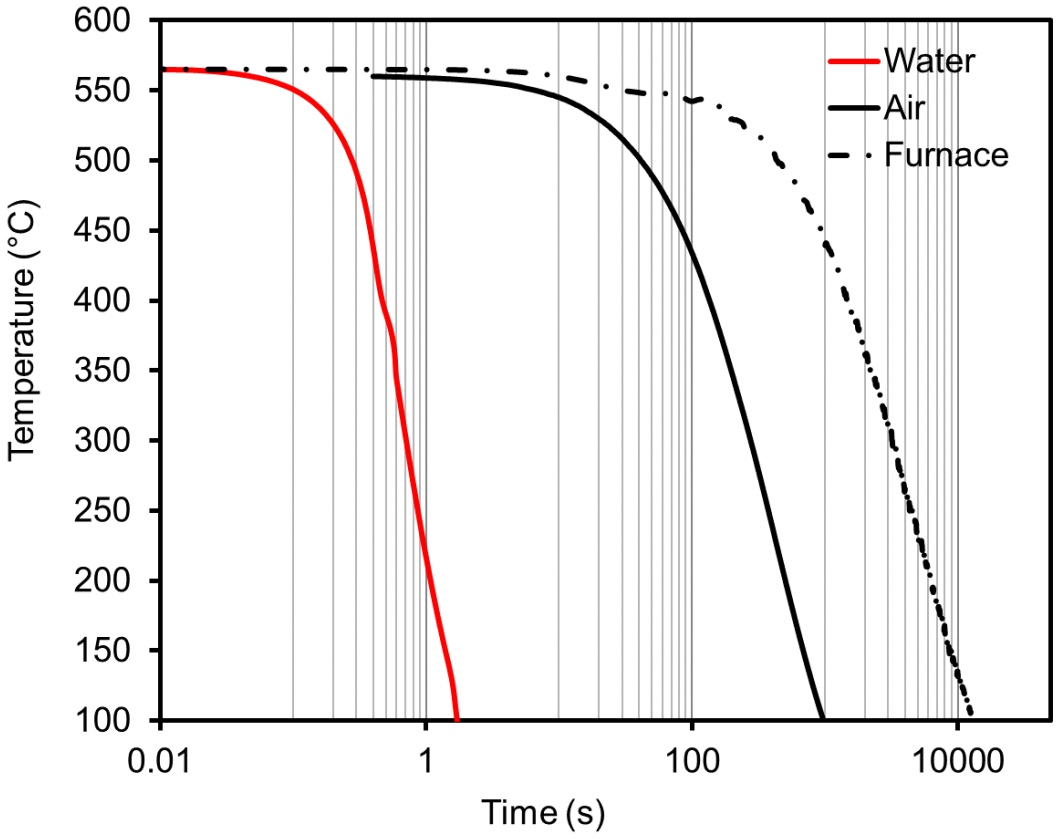

Figure 5-6: Time temperature curves plotted on a logarithmic scale showing the difference in cooling between the water (394.6°C/s), air (0.727°C/s), and furnace (0.0605°C/s) cooled samples

Using the same procedure as for the Jominy quenched end bar, average cooling rates from 500-250°C were also calculated for these tests. The data shown in Figure 5-6 shows extremely fast cooling of the sample for the water quenched case (cooling rates of ~390°C/s) in contrast the air

cooled sample had an average cooling rate of 0.73°C/s and the furnace cooled sample was cooled orders of magnitude slower at an average cooling rate of 0.0605°C/s.

Figure 5-6 is plotted on a logarithmic scale, the difference in cooling for the three conditions is exponentially different. These tests were designed to capture cooling that could not be achieved using a Jominy bar, and to provide samples for subsequent tensile testing.

5.3 Hardness Profile of AA6063

The hardness profile is the hardness data collected from the Jominy bar, plotted against the distance from the quenched end of the Jominy bar. Figure 5-7 shows the results of the results of the Jominy end quench test in the form of a hardness profile.

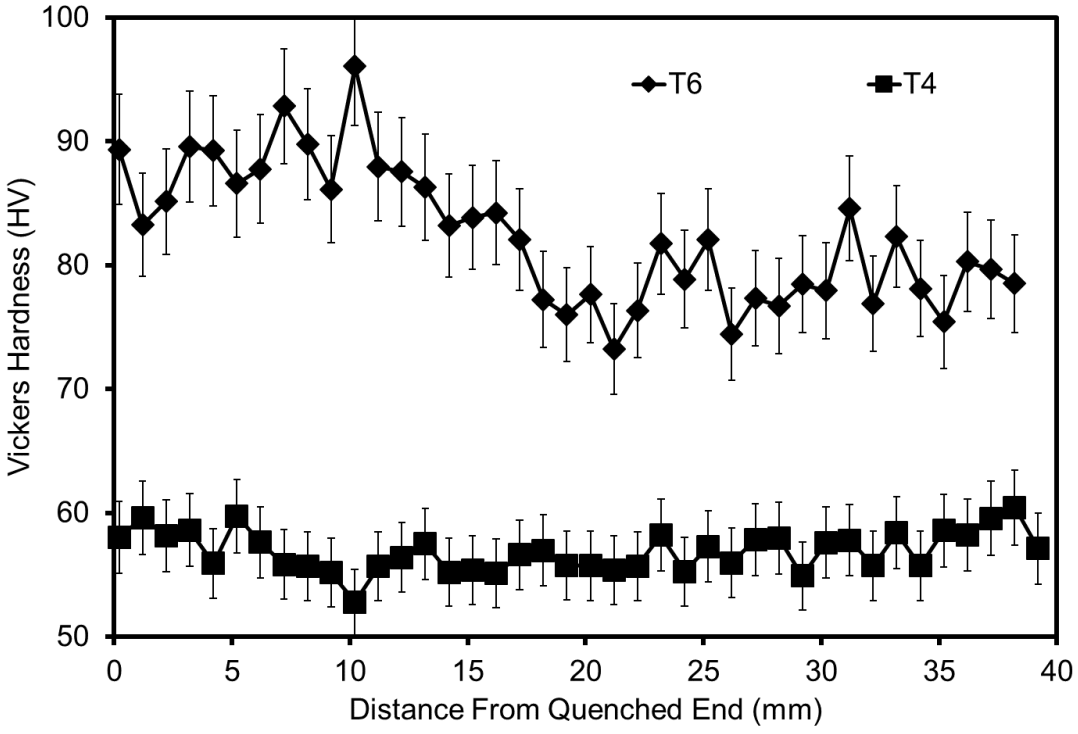

Figure 5-7: Measured hardness profiles along the Jominy quench bar for AA6063

The results of this experiment show that as the distance from the quench end increases, and subsequently the cooling rate decreases, then the hardness of the alloy remains fairly stable

for the T4 condition but goes down slightly in the T6 condition. As shown in this figure, the hardness of AA-6063 alloy was not particularly quench sensitive. As seen in Figure 5-7 the difference between the quenched end and the furthest point there is only ~11 HV.

5.3.1 Hardness vs. Cooling Rates

The Jominy test provided a range of cooling rates, however the Jominy bar was unable to provide cooling rates that significantly changed the properties after approximately 40 mm from the quenched end. To further the understanding of the mechanical behaviour of these alloys with respect to quench sensitivity, a test was designed that measure more extreme cooling rates and provide larger samples for tensile testing. The hardness with respect to the cooling rate was investigated under the three conditions, water cooled, air cooled, and furnace cooled. Figure 34 shows the results of the hardness plotted against the three different average cooling rates for the baseline alloy.

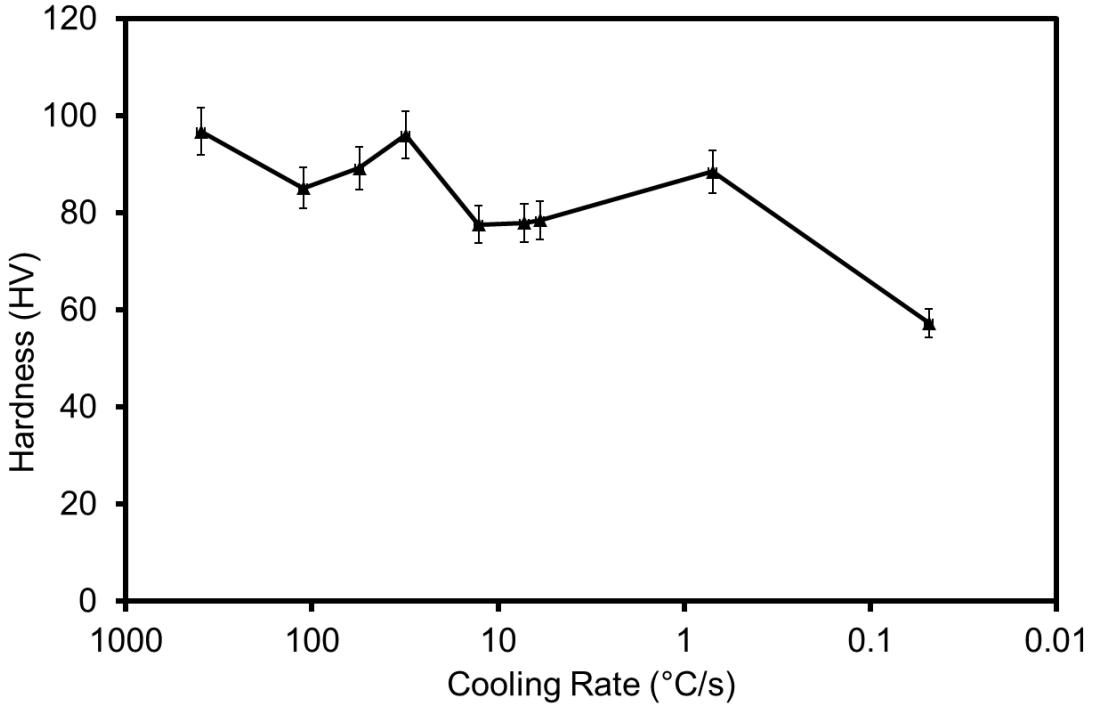

Figure 5-8: Measured hardness profile as a function of average cooling rate using both selected Jominy bar locations and the other cooling tests for AA6063 in the T6 condition – cooling rates: water – 394.6°C/s, air – 0.727°C/s, and furnace – 0.0605°C/s

The above figure shows the measured hardness results from both the Jominy test and other cooling tests in the form of hardness plotted against the cooling rate. As expected with the AA6063, the alloy does not appear to be very quench sensitive until the cooling rate drops below 0.8°C/s.

5.4 Effect of alloy composition

5.4.1 Hardness Profiles

The same Jominy quench tests were done for AA6xxx alloys C1 and C3. The results of the Jominy quench test for each of these alloys are shown in Figure 5-9 in the form of a hardness profile for the alloys in the T4 condition.

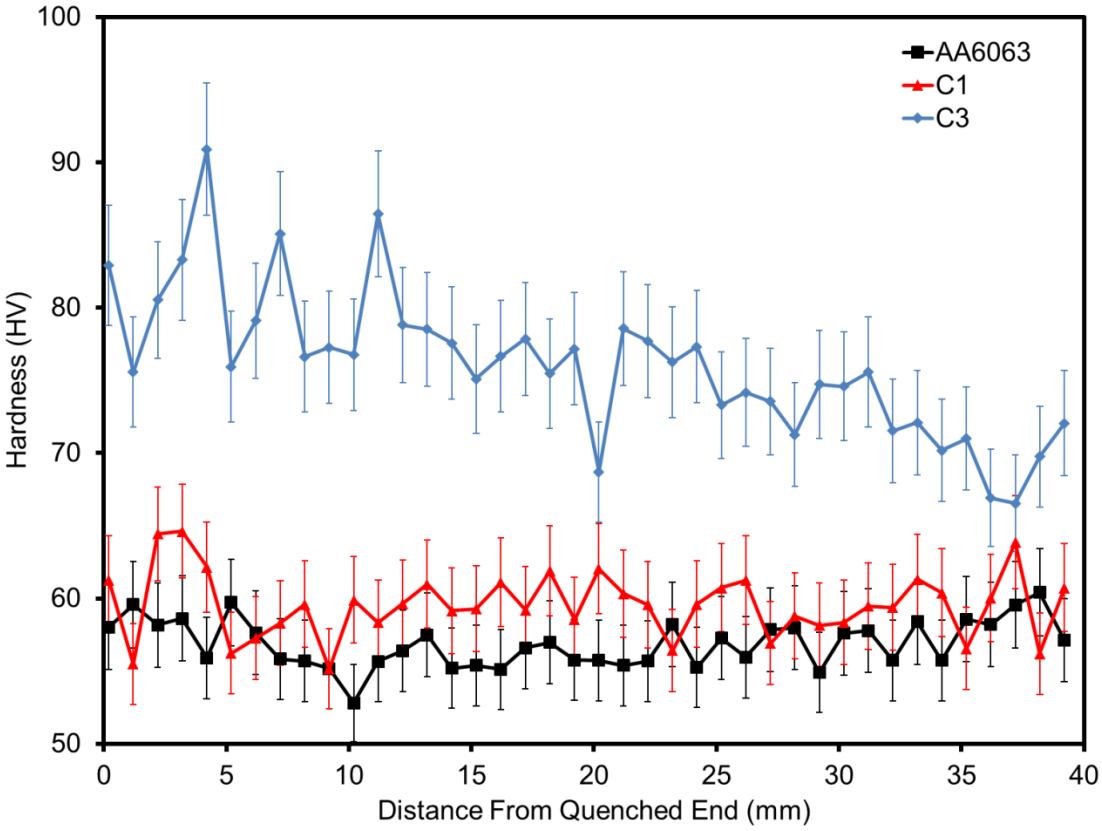

Figure 5-9: Measured hardness profile along the Jominy bars for all the alloys studied in the T4 temper

Referring to Figure 5-9, it is apparent that alloy C3 exhibits the highest hardness and also appears to be more quench sensitive in the T4 condition than either alloy C1 or AA6063. Alloy C1 and AA6063 appear to have a similar hardness in the T4 condition

This research indicates that the alloy composition in particular the amount of transition elements (Cr and Mn) play a large role in the quench sensitivity of AA6xxx aluminum alloys. In addition, as expected the amount to Mg and Si determine the overall hardness of the alloy. The transition metals play a large role in quench sensitivity as higher levels of these alloy additions can lead to larger dispersoid densities for a given homogenization treatment and is known to be one of the key factors that affects the quench sensitivity of an alloy. In fact, other research has

shown that there is a direct proportional relationship between the two for AA6xxx series aluminum alloys processed under equivalent conditions [5-8].

At industrially relevant cooling rates, dispersoids act as precipitation sites for non-hardening Mg-Si-containing phases and hence promote solute loss. This precipitation can also take place at other precipitation sites such as grain boundaries and/or dislocation lines. Although, due to their lower distribution, nucleation on these sites is less common.

AA6xxx series extrusion alloys all contain dispersoids that are very similar in their size and composition. The size, composition and crystal structure of dispersoids are determined by the homogenization treatment and the alloy composition, in particular the transition metal (Cr and Mn) content. For transition metal contents typical in the alloys investigated (Mn < 0.3wt.%, Cr < 0.3wt.%) all dispersoid phases are based on the primary intermetallic phases $Al_{12}Fe_3Si$ or $Al_{15}Mn_3Si_2$. This means that all dispersoids have a cubic unit cell with the cell parameter a=1.26nm [40], so that the interfacial energy is expected to be very similar. The potential of each single dispersoid to act as a nucleation site is hence the same, particularly since the size of the dispersoids are probably very similar after the same homogenization treatment (560°C for 6 hours) independent of the alloy composition. Consequently, it can be assumed that the nucleation kinetics would probably be the same in each of the alloys. Therefore, it is expected that all dispersoids present under the conditions described above have the same potential as nucleation sites for the Mg-Si phases.

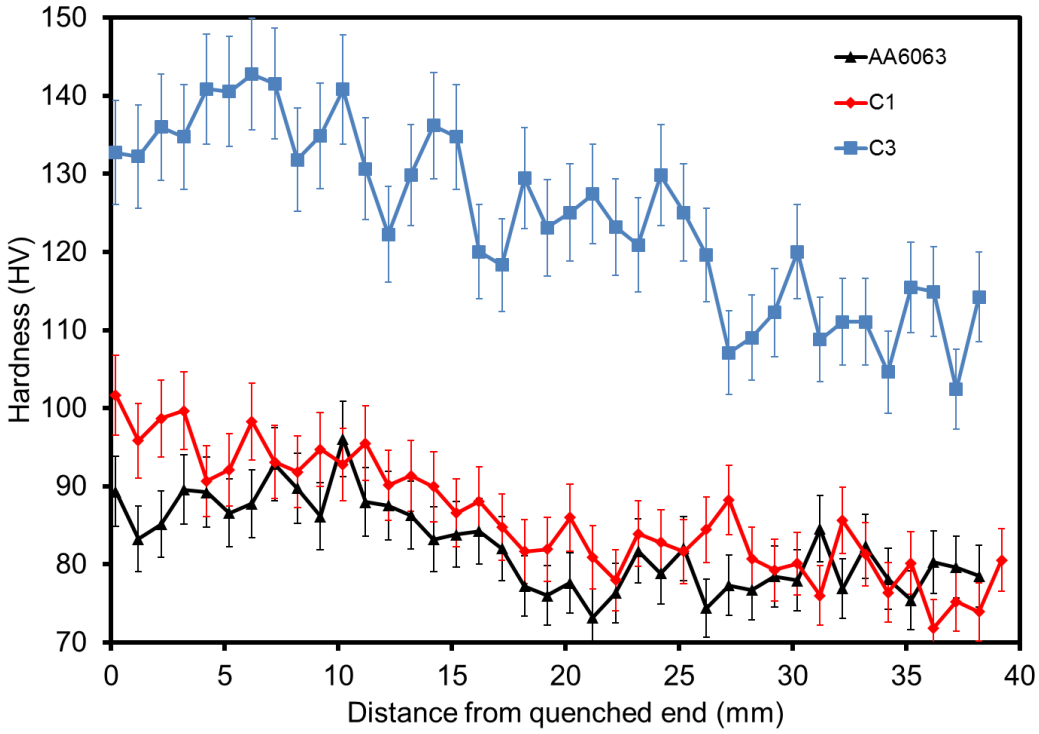

Figure 5-10: Measured hardness profiles along the Jominy quench bar for all the alloys studied in the T6 condition; comparison between C1, C3, and baseline alloys, all in the T6 condition

Figure 5-10 shows that once the Mg_2Si comes out of solution during quenching, the subsequent aging procedure results in overaged precipitates which are non hardening phases. Once the alloy was aged, quench sensitivity, though minimal, was observed in AA 6063. The results shown in Figure 5-10 show that the effect of adding Cr to a AA6xxx aluminum alloy (C1 and C3). These alloys exhibit more quench sensitivity then the baseline AA6063. The large change in mechanical properties as a function of cooling rate is likely due to precipitation of Mg_2Si on dispersoids in the matrix. The data does show some scatter; however, the overall trend is down as the distance from the quenched end increases. The difference in HV between the highest hardness and lowest hardness is ~ 30 HV, a relatively large number. The same pattern was observed in Figure 5-10, showing that precipitation of Mg_2Si during the quenching operation greatly affects the age hardening response of the alloy. C1 showed an alloy with similar Mg

concentration to the baseline alloy, but increased amounts of Cr. C3 is an alloy that contains increased amounts of both Mg and Cr. The reason for comparing C1 and C3 is to prove that the increased quench sensitivity is in fact coming from the added Cr and Mn, while some may be coming from added Mg. The results of the Jominy quenched end test shown in the hardness profile in Figure 5-10 shows a similar result to the one observed in C1. The difference in hardness between the closest point to the quenched-end and the furthest point is ~29 HV.

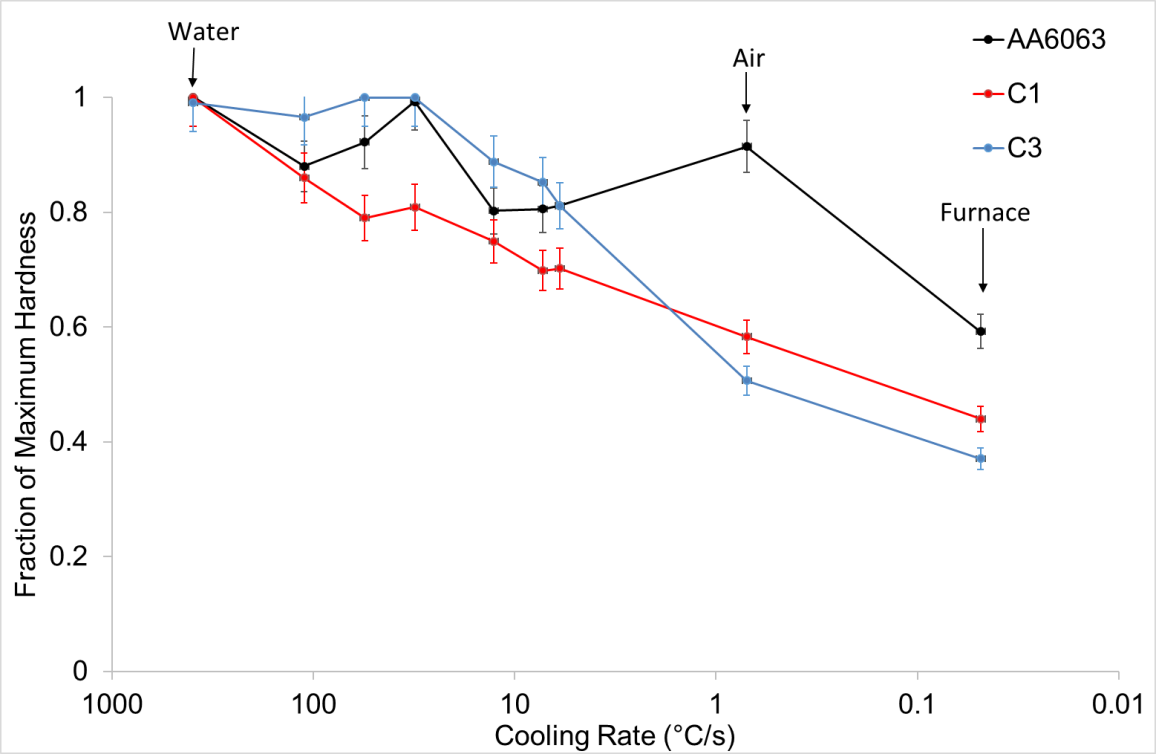

Figure 5-11: Normalized hardness profiles along the Jominy quench bar for all the alloys studied in the T6 condition; comparison between C1, C3, and baseline alloys, all in the T6 condition –

The results shown in Figure 5-11 also compare the normalized hardness profiles to compare the change from the maximum hardness as the distance from the quenched end increased. This shows that the increase in Cr and Mn is one of the reasons responsible for the increase in quench sensitivity and the increase in Mg, which has an increase on the overall hardness of the alloy, does not affect quench sensitivity significantly. The increase in hardness due to the added Mg is no longer apparent when the cooling rate is ~1 °C/s. At this cooling rate

the added Mg no longer hardens the alloy. Figure 5-11 compares the quench sensitivity of the three alloys based on the results from the Jominy quenched end test and the other cooling tests. Both C1 and C3 have similar trends and progress down in a similar manner. The two alloys show agreement in their quench sensitivity and as expected, the two alloys have similar quench sensitivity. C1 and C3 are the two alloys containing higher amounts of Cr and Mn, while the baseline alloy does not contain Cr and has a lower amount of Mn. The baseline alloy has a more level progression downwards as the distance from the quenched end increases. C1 and the baseline 6063 alloy have similar Vickers Hardness but the difference between the hardness at the quenched end and at the point furthest from the quenched end are different for the two alloys.

5.4.2 Hardness vs. Cooling Rate

To extend the cooling rates further, other cooling tests were combined with the results from the Jominy bar in Figure 5-12.

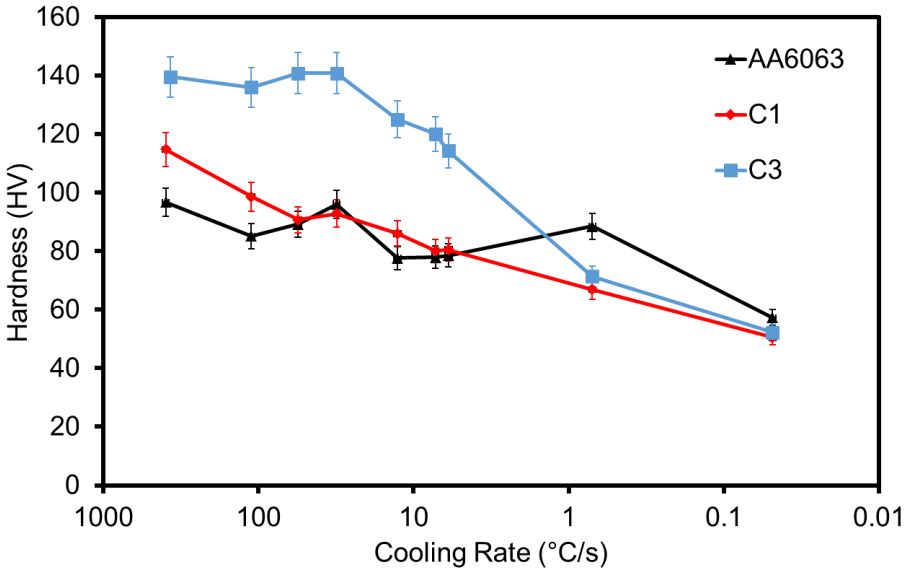

Figure 5-12: Extended hardness profile showing data obtained from extreme cooling tests and Jominy bar combined for all three alloys, all hardness measurements were taken in the T6 condition and all cooling rates are averages

The baseline alloy at a cooling rate of approximately 0.8°C/s had a Vickers hardness of 88 HV, the C1 alloy containing a similar composition with increased amounts of Cr had a Vickers hardness of 67 HV at the same average cooling rate. The baseline alloy did not decrease in strength the same way that C1 did, the decrease in hardness becomes even more dramatic if the percent decrease in hardness is taken into consideration. C1 was harder after the water quench, at 114 HV the C1 alloy was 18 HV harder than the baseline alloy, which was at 96 HV. The increased Cr caused the alloy to go from 18 HV harder after the water quench to 14 HV softer than the baseline alloy after the air cooling. A similar trend was seen in the C3 alloy as the C1 alloy, however the quench sensitivity was even greater in this alloy because the hardness was 140 HV after the water quench.

When the alloy reached approximately 0.8°C/s, the HV of the C3 alloy became 71 HV. The results shown in Figure 5-12 show a similar pattern for both C1 and C3 alloys. However, both C1 and C3 differ from the results of the AA6063 alloy, and are more quench sensitive due to the addition of Cr to the composition. The most important points for comparison are the two cooling rates of ~370°C/s and ~0.8°C/s. These two values correspond to the water and air cooling rates respectively.

When looking at these two important cooling rates in Figure 5-12, it can be seen that at the fastest cooling rate, C3 is the hardest, then C1, and baseline is the weakest. Comparing this to the much slower cooling rate of 0.8°C/s, the baseline alloy at this cooling rate is the hardest, and C3 and C1 have similar values. The addition of Cr and Mn as seen in these results, greatly affects the age hardening response when the alloy is quenched too slowly. Quenching fast allows Mg and Si to remain in solution, however quenching more slowly allows Mg_2Si to begin

precipitating during the quench. The addition of Cr and Mn appears to increase the ability of Mg_2Si to precipitate during the quenching operation probably due to the increased number of dispersoids and nucleation sites for the Mg2Si to precipitate on.

5.4.3 Stress vs. Strain

The results from the tensile tests can be converted into stress-strain curves and the data may be represented as one of these curves. The yield stress, ultimate tensile stress (UTS) elongation, toughness, and fracture stress can all be found from the stress-strain curve. The stress-strain curve for the C3 alloy in the T6 condition that was water quenched is shown in Figure 5-13.

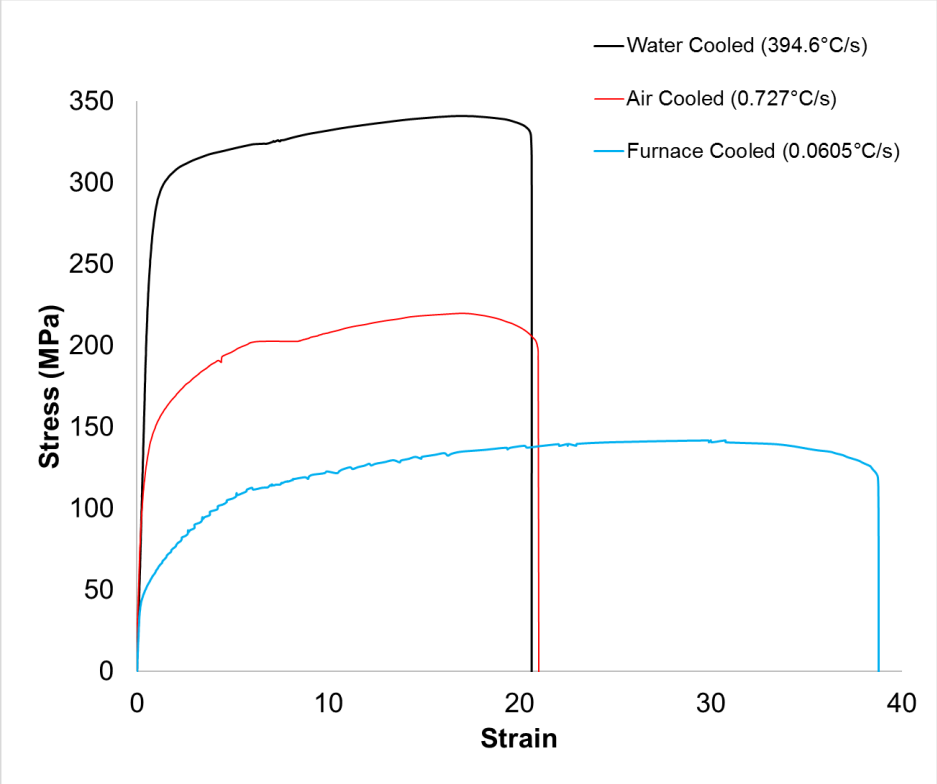

Figure 5-13: Measured stress-strain curves for AA6xxx alloy C3 that was water, air, and furnace cooled after solution treatment, and then aged to a T6 temper

The yield stress and UTS seen for C3 water quenched (C3W) T6, are relatively large compared to those seen in the C3 air cooled (C3A) T6 condition. The C3W condition had the fastest cooling rate and there for resulted in the highest yield strength and UTS. The yield strength and UTS seen in C3 furnace cooled (C3F) T6, as expected are lower than those observed in C3A T6. The elongation in C3A T6, appears to be only slightly larger than the elongation in C3W T6. It was expected that the strain would be slightly larger than the strain in C3F T6, this result was exactly as expected. A low yield strength, and a low UTS were expected from an alloy that quenched extremely slowly. The elongation in C3F T6 was also as expected, the ductility of the sample dramatically increased from the C3W T6 samples. According the results seen for these three conditions, quench sensitivity due to the addition of Cr and Mn to the AA6xxx alloys, increased greatly, affecting the mechanical properties obtained from the stress-strain curve. This was observed by the large decreases in both yield strength and UTS as the cooling rate got slower.

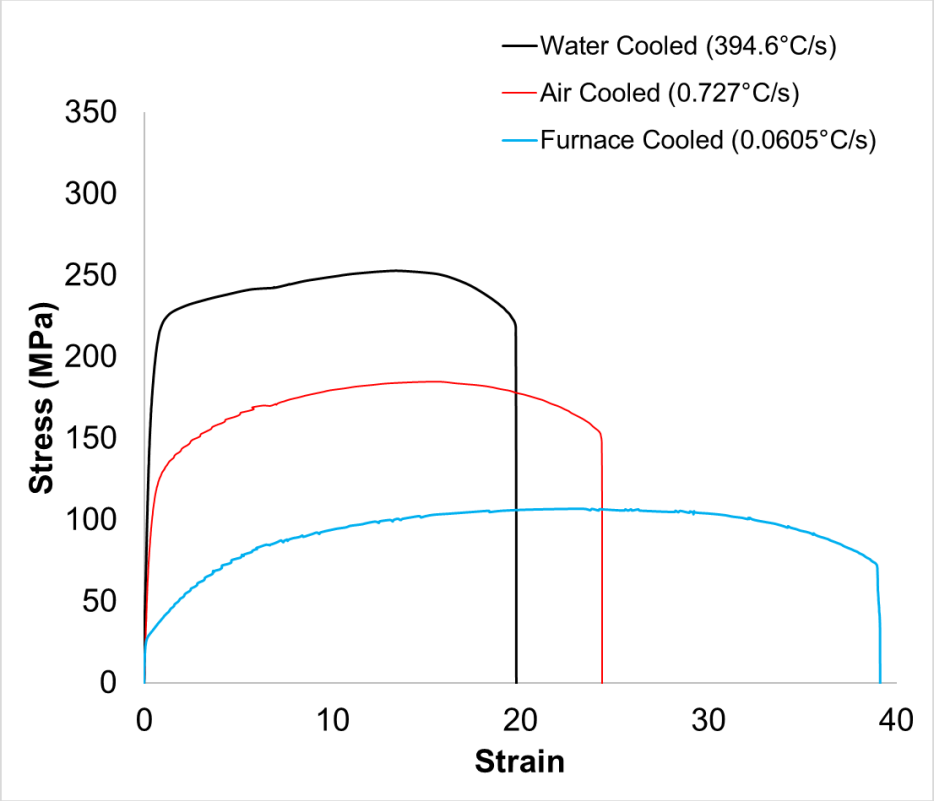

Figure 5-14: Measured stress-strain curves for AA6xxx alloy C1 that was water, air, and furnace cooled after solution treatment, and then aged to a T6 temper

To compare and show the effect of cooling rate on various mechanical properties. The stress-strain curves for alloy C1 under the three different cooling conditions were plotted on the same graph for visual comparison. Figure 5-14 shows the graph of all three stress-strain curves, showing a clear relationship between the quenching condition and the mechanical properties of the alloy. C1W T6 had a relatively high yield strength, and UTS. This shows that the water quenched specimens have undergone the least Mg_2Si precipitation during quenching. This was seen in the mechanical properties after aging. By not allowing Mg_2Si to precipitate out of the supersaturated solid solution during quenching, more Mg_2Si is available to transform into the β" hardening precipitates. The addition of Cr, increases the likely hood that Mg_2Si will precipitate during slower quenches causing quench sensitivity. The slower cooling rates as a result of air cooling, caused C1A T6 to have a lower yield strength, and UTS than the water quenched sample

seen in Figure 5-14. The ductility as expected increased in the air cooled sample. C1F T6 was cooled slower than C1A T6, and the difference in the stress-strain relationship when quenched under these conditions was shown in Figure 5-14. The results from this test for C1F T6 shown in figure 43 show that by cooling even slower than air, the yield strength and UTS continue to go down while the ductility continues to increase. The cooling rate during the furnace quench was extremely slow. Like the results seen in Figure 5-13 with the C3F T6 alloy, this C1F T6 alloy shows that the cooling rate affects the mechanical properties after aging. Like the other Cr containing alloy C3, C1 also exhibits increased quench sensitivity.

5.4.4 Yield Stress vs. Cooling Rate

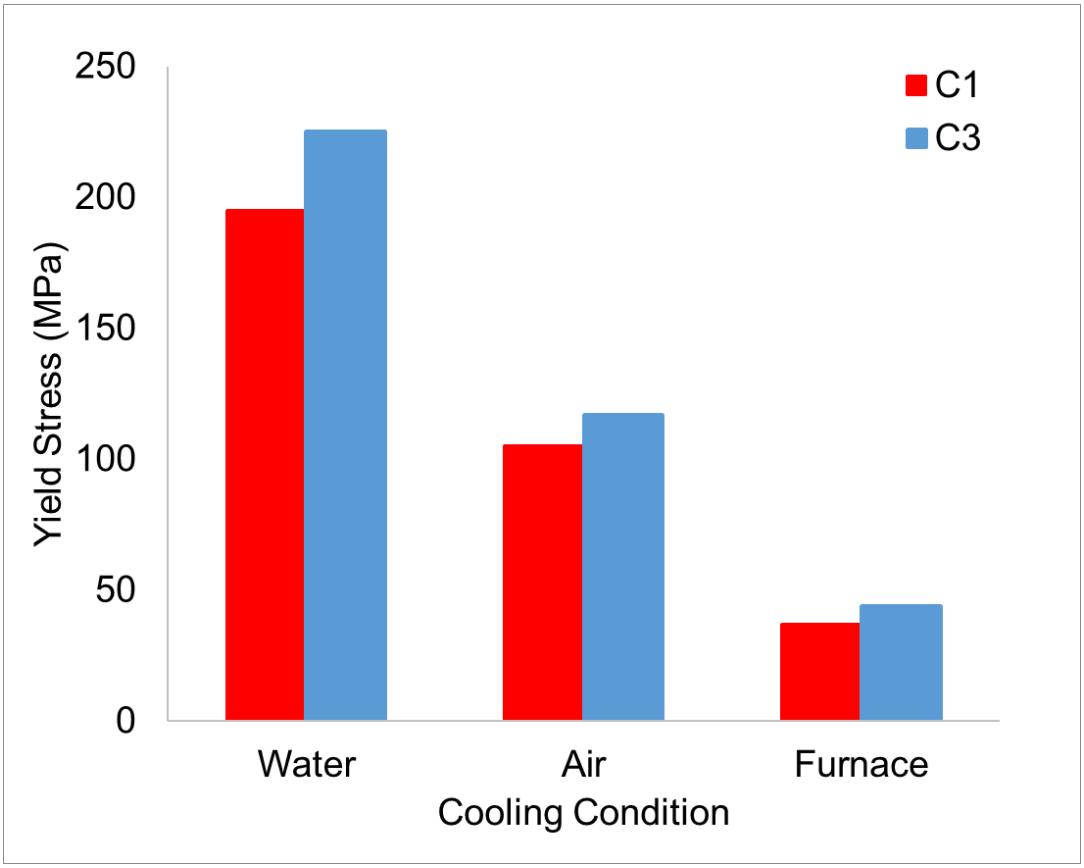

Figure 5-15: Measured yield strengths plotted against the cooling rate during quenching of the AA6xxx alloys C1 and C3 alloys, all samples were in the T6 condition

The yield stresses of three different tensile samples that were all made from the C1 alloy and in the T6 condition were plotted against their respective cooling condition in Figure 5-15. Based on the results shown in Figure 5-15, the yield stress had a strong correlation with the cooling rate during the quench after the solution treatment. As the cooling rate increased, the yield stress also increased. The difference in yield strength for this alloy between the water and furnace cooled samples was large. The furnace-cooled sample was 18.7% of the strength of the water-cooled sample. The percent difference in strength between the water-cooled sample and the furnace-cooled sample was 81.3%.

Figure 5-15 also shows the yield stress plotted against the cooling rate, for the C3 alloy, all samples were in the T6 condition. The difference in yield strength for this alloy between the water and furnace cooled samples was large in C3. The furnace-cooled sample was 19.6% of the strength of the water-cooled sample. The percent difference in strength between the water-cooled sample and the furnace-cooled sample was 80.4%. The percent difference in yield strength between both Cr containing alloys was almost identical.

5.4.5 UTS vs. Cooling Rate

The ultimate tensile strength is another mechanical property that may be affected by quench sensitivity. From the data obtained from the tensile tests, the UTS of each sample condition was taken and plotted against the cooling rate during the quench after the solution treatment. This was done in order to show the effect of the cooling rate during quenching on the UTS.

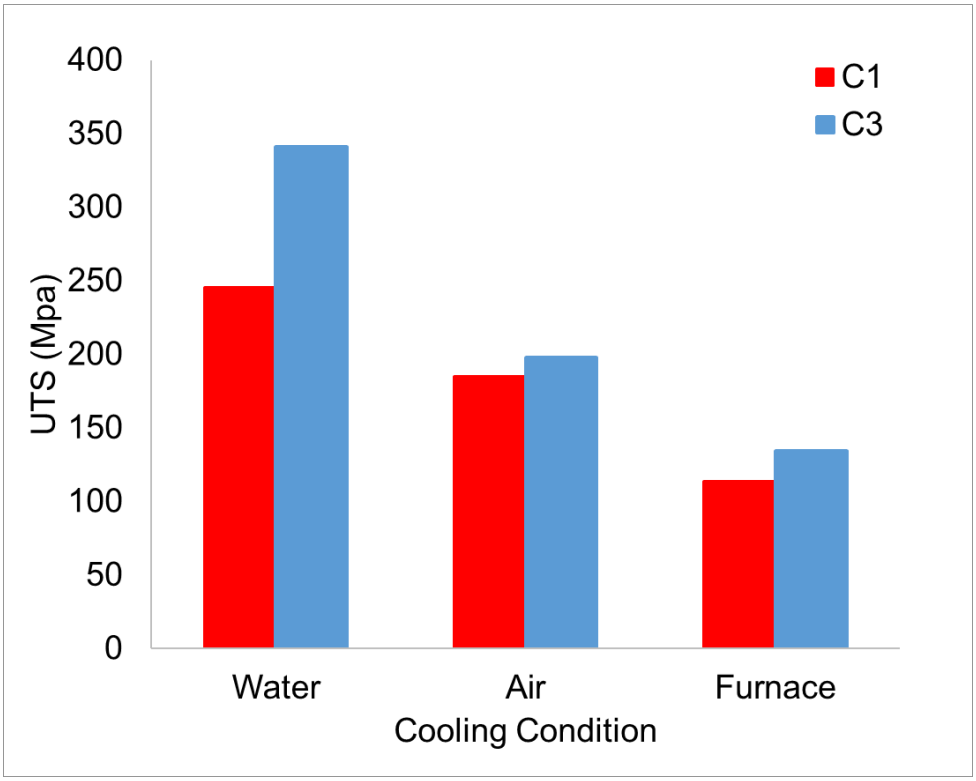

Figure 5-16: Measured ultimate tensile strengths plotted against the cooling rate during quenching of the AA6xxx alloys C1 and C3 alloys, all samples were in the T6 condition

Figure 5-16 shows the UTS plotted against the cooling rate during quenching. The UTS increases as the cooling rate increases. Based on the results shown in Figure 5-16, there is a positive correlation between UTS and cooling rate. It should be noted that the cooling rate was plotted using a logarithmic scale. The lowest cooling rate of ~0.06°C/s had a UTS of 113.9 MPa, while the highest cooling rate of ~370°C/s had a UTS of 245.5 MPa in the C1 alloy. The furnace cooled or slowest cooled sample had a UTS that was 46.4% of the strength of the fastest cooled or water cooled sample. This gives a percent difference of 54.6% between the water cooled and furnace cooled sample. Figure 5-16 also shows the results from the tensile tests for the C3 alloy in the T6 condition. The UTS was plotted against the cooling rate. The cooling rate was plotted using a logarithmic scale. Figure 5-16 shows that the UTS increases as the cooling rate increases, similar to the results observed for C1. The lowest cooling rate of ~0.06°C/s had a UTS of 134.4

MPa, while the highest cooling rate of ~370°C/s had a UTS of 341.2 MPa for the C3. The furnace cooled or slowest cooled sample had a UTS that was 39.4% of the strength of the fastest cooled or water cooled sample. This gives a percent difference of 60.6% between the water cooled and furnace cooled sample. This differed slightly from the results observed for C1, there was a 6% difference in strength between the two percent differences. This was likely due to the fact that C3 had a high Mg content which affected the strength of the alloy. In both alloys there was a major change in strength based on the cooling rate, the two alloys had a slightly different response due to the role Mg plays in work hardening.

5.4.6 Elongation vs. Cooling Rate

Elongation is a measure of ductility in materials. The effect of cooling rate during quenching on the ductility of alloy was studied by plotting the percent elongation against the cooling rate.

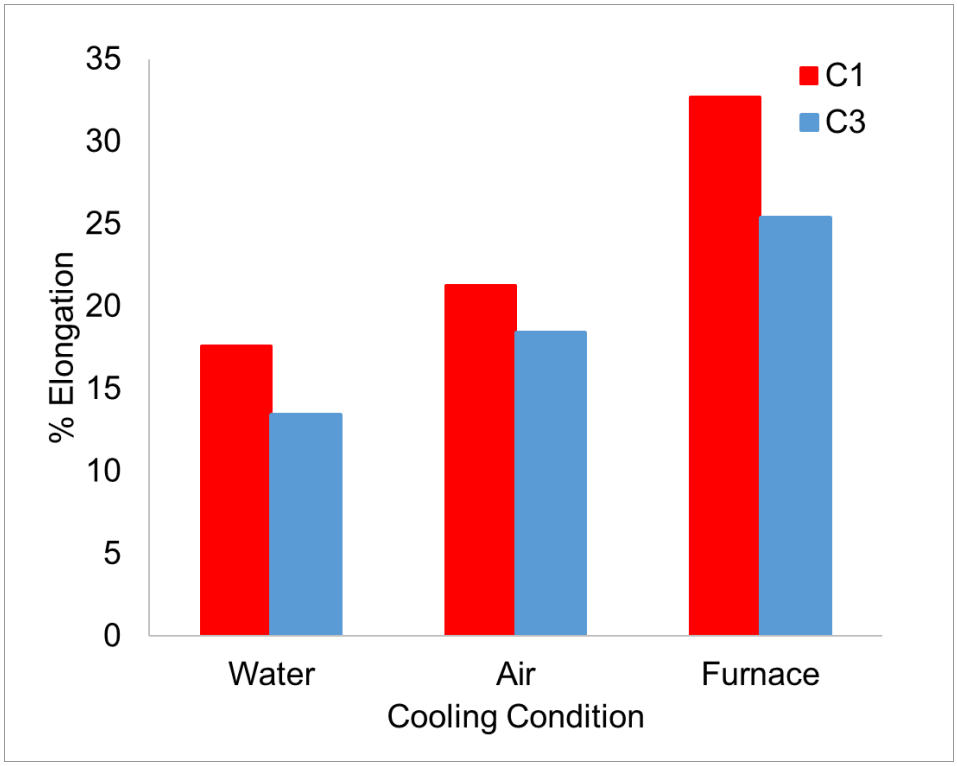

Figure 5-17: Measured percent elongation versus cooling rate during quenching of the AA66xx C1 and C3 alloys, after age hardening in the T6 condition

The percent elongation decreases as the cooling rate increases. Figure 5-17 shows that the ductility of the material decreases as the cooling rate increases. This result was expected because typically materials that have larger yield strengths and ultimate tensile strengths, typically have lower percent elongations. The plastic behaviour of materials usually follows this pattern, and as seen in previous figures the cooling rate plays a large role in the strength of both C1 and C3 alloys. The results shown in figure 5-17 indicate that C3 follows a similar pattern to C1 with respect to percent elongation. The percent elongation however in the C3 alloy is affected by the increased Mg of the alloy resulting in smaller percentages of percent elongation than observed in C1.

5.4.7 Scanning Electron Microscopy

To characterize the microstructure and look for the differences in microstructure between specimens that were slow cooled and specimens that were rapidly cooled in water, an SEM was

used to image the samples. These samples were imaged in the as quenched condition, meaning that they were not aged. The goal of this was to look for precipitation that may have occurred during quenching, if the samples were aged, only precipitates after aging may have been seen, however β" hardening precipitates are too small to be seen in the SEM. Equilibrium phase Mg_2Si is large enough for viewing in the SEM.

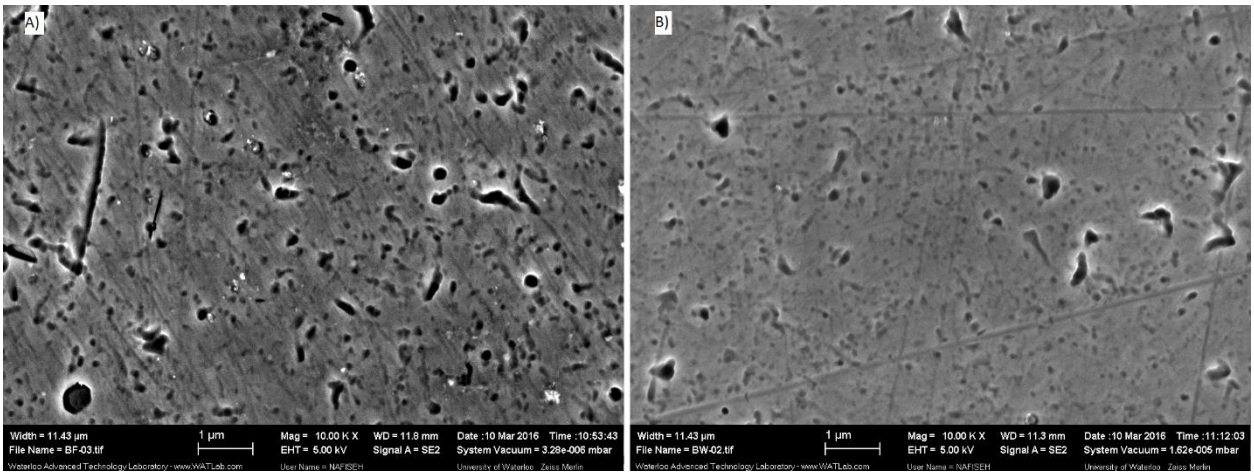

Figure 5-18: Scanning electron micrograph of as quenched baseline 6063 alloy at 10.00K x magnification and 5.00 kV, a) sample in furnace quenched condition, b) Sample in water quenched condition

Image "A" in Figure 50 shows the AA6063 alloy after being furnace cooled, while image "B" shows the same alloy after being water quenched. The furnace quenched sample appears to have larger phases due to the aggregation of precipitates during the quenching process. This microstructure shows how the quench rate can affect the over all mechanical properties. The smaller particles seen in image "B" result in an alloy with higher yield strength, and UTS. The smaller particles seen in image "B" can be attributed to higher amount of Mg_2Si remaining in that solid solution.

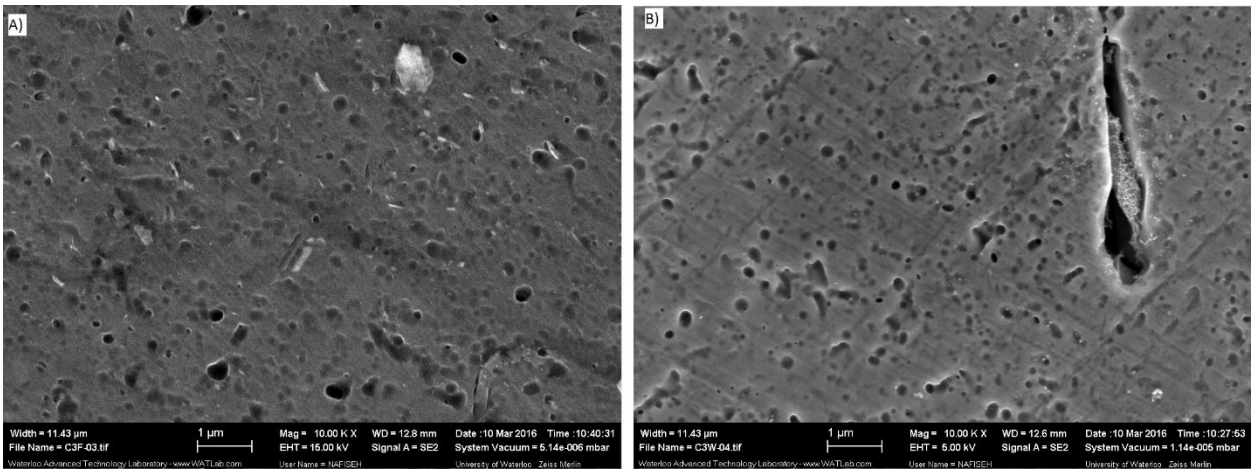

Figure 5-19: Scanning electron micrograph of as quenched C3 alloy at 10.00K x magnification, 15.00kV and 5.00 kV, a) sample in furnace quenched condition, b) Sample in water quenched condition

The images shown in Figure 5-19 are the SEM micrographs of the C3 alloy. Image "A" is in the furnace quenched condition and had the lowest strength. Image "B" is in the water quenched condition, and had the highest strength. The image in B appears to have a more defined microstructure, where as the image in A appears to contain larger precipitates. This may be contributing to the weakened state of the alloy.

6 Conclusions and Suggested Work

This research shows that the alloy content in AA6xxx alloys, in particular the transition metal content (Cr and Mn) which lead to different dispersoid densities, plays a significant role in quench sensitivity. This is mainly due to dispersoids acting as precipitation sites for the non-hardening β -Mg_2Si phase, leading to solute loss and a reduced amount of Mg and Si available for subsequent precipitation hardening. These results confirm the general knowledge about quench sensitivity and the role dispersoids play during the process.

Various laboratory experiments including the Jominy quenched end test, tensile test, and scanning electron microscopy were conducted. Three different alloys were tested, AA6063, Composition 1, and Composition 3, where these compositions were AA6063 alloys with added alloying elements. Compositions 1 and 3 were both chromium containing alloys, but also had higher levels of Mn and the objective this thesis was to find out the quench sensitivity of each of these alloys. After conducting these tests several conclusions can be drawn:

I. The AA6063 exhibited minimal quench sensitivity and can tolerate relatively slow cooling rates after solutionizing but still get close to peak aged strength.

II. The addition of chromium and manganese to AA6xxx aluminum alloys causes an increase in quench sensitivity as seen with composition 1 and 3. The hardness of composition 1 in the air cooled condition was ~67 HV while the baseline 6063 alloy was 88 HV. There was ~21 HV difference between composition 1 and the baseline alloy quenched at the same rate, and the only major difference in their composition was the addition of chromium.

Both compositions 1 and 3 exhibit the same level of quench sensitivity and this appears to be related to the Cr and Mn levels in these alloys. Both alloys followed the same

trends in the Jominy results with about the same level of quench sensitivity. Composition 1 had a difference of ~30 HV between the fastest and slowest cooled points along the Jominy bar. Composition 3 had a difference of ~29 HV between the fastest and slowest cooled points along the Jominy bar. To improve on the findings found in this thesis, an in depth transmission electron microscopy study should be conducted. A TEM study will greatly increase the knowledge of how dispersoids affect the quench sensitivity of AA6xxx aluminum alloys. Due to the small size of β" precipitates, it was difficult to see the precipitates and measure precipitate density when viewing under the SEM. The SEM also did not have a high enough resolution to accurately conduct an EDS scan on a chromium containing dispersoid. Without doing this it is impossible to do a complete microstructural analysis that would benefit this study.

This study looked at homogenized samples but the effect of grain structure both smaller recrystallized grains and a fibrous structure more typical of extruded profiles and the effect this has on quench sensitivity would also be of interest to study. Another interesting study would be to create samples via homogenization with no dispersoids and see if they exhibit any quench sensitivity.

7 References

[1] Courtesy Figure developed by Professor Warren Poole at the University of British Columbia

[2] Mrówka-Nowotnik, Grażyna, and Sieniawski. "Influence of Heat Treatment on the Microstructure and Mechanical Properties of 6005 and 6082 Aluminium Alloys." *Journal of Materials Processing Technology* 162-163 (2005): 367-72.

[3] Esmaeili, Shahrzad, and D. J. Lloyd. "Characterization of the Evolution of the Volume Fraction of Precipitates in Aged AlMgSiCu Alloys Using DSC Technique." *Materials Characterization* 55.4-5 (2005): 307-19.

[4] Mohamed, A.m.a., and F.h. Samuel. "A Review on the Heat Treatment of Al-Si-Cu/Mg Casting Alloys." *Heat Treatment - Conventional and Novel Applications* (2012).

[5] Lodgaard, L. *Precipitation of Dispersoids Containing Mn And/ or Cr in Al-Mg-Si Alloys*. Thesis. Norwegian University of Science and Technology, 2000.

[6] Lodgaard, L. and N. Ryum. "Precipitation of Dispersoids Containing Mn And/or Cr in Al–Mg–Si Alloys." *Materials Science and Engineering: A* 283.1-2 (2000): 144-52.
[7] Sheppard, T. "Press Quenching of Aluminium Alloys." *Materials Science and Technology* 4.7 (1988): 635-43.

[8] Dons, A.l., and O. Lohne. "Quench Sensitivity of Almgsi-Alloys Containing Mn or Cr." *MRS Proc. MRS Proceedings* 21 (1983).

[9] Li, Y.j., and L. Arnberg. "Quantitative Study on the Precipitation Behavior of Dispersoids in DC-cast AA3003 Alloy during Heating and Homogenization." *Acta Materialia* 51.12 (2003): 3415-428.

[10] Azarbarmas, Mortaza, M. Emamy, J. Rassizadehghani, M. Alipour, and M. Karamouz. "The Influence of Beryllium Addition on the Microstructure and Mechanical Properties of Al–15%Mg2Si In-situ Metal Matrix Composite." *Materials Science and Engineering: A* 528.28 (2011): 8205-211.

[11] "Online Materials Information Resource - MatWeb." *Online Materials Information Resource - MatWeb*. Web. 25 Mar. 2016.

[12] Porter, D. A., K. E. Easterling, and M. Y. Sherif. *Phase Transformations in Metals and Alloys*. Boca Raton, FL: CRC, 2009.

[13] Asensio-Lozano, Juan, B. Suárez-Peña, and G. Vander Voort. "Effect of Processing Steps on the Mechanical Properties and Surface Appearance of 6063 Aluminium Extruded Products." *Materials* 7.6 (2014): 4224-242.

[14] Bratland, D. H., Ø. Grong, H. Shercliff, O.r. Myhr, and S. Tjøtta. "Overview No. 124 Modelling of Precipitation Reactions in Industrial Processing." *Acta Materialia* 45.1 (1997): 1-22.

[15] Bratland, D. H. "Process Model Based Alloy Design and Optimisation of Cooling Schedules for Al-Mg-Si Extrusions." Thesis. University of Trondheim, 1995.

[16] Li, Hong-Ying, Cui-Ting Zeng, Mao-Sheng Han, Jiao-Jiao Liu, and Xiao-Chao Lu. "Time–temperature–property Curves for Quench Sensitivity of 6063 Aluminum Alloy." *Transactions of Nonferrous Metals Society of China* 23.1 (2013): 38-45.

[17] Shang, B.c., Z.m. Yin, G. Wang, B. Liu, and Z.q. Huang. "Investigation of Quench Sensitivity and Transformation Kinetics during Isothermal Treatment in 6082 Aluminum Alloy." *Materials & Design* 32.7 (2011): 3818-822.

[18] Staley, J. T. "Quench Factor Analysis of Aluminium Alloys." *Materials Science and Technology* 3.11 (1987): 923-35.

[19] Steele, D., D. Evans, P. Nolan, and D.j. Lloyd. "Quantification of Grain Boundary Precipitation and the Influence of Quench Rate in 6XXX Aluminum Alloys." *Materials Characterization* 58.1 (2007): 40-45.

[20] Tanner, D. A., and J. S. Robinson. "Residual Stress Magnitudes and Related Properties in Quenched Aluminium Alloys." *Materials Science and Technology* 22.1 (2006): 77-85.

[21] Tiryakioğlu, Murat, and R. T. Shuey. "Quench Sensitivity of an Al-7 Pct Si-0.6 Pct Mg Alloy: Characterization and Modeling." *Metallurgical and Materials Transactions B* 38.4 (2007): 575-82.

[22] Reiso, Oddvin, Hilde-Gunn Øverlie, and N. Ryum. "Dissolution and Melting of Secondary Al2Cu Phase Particles in an AlCu Alloy." *MTA Metallurgical Transactions A* 21.6 (1990): 1689-695.

[23] Myhr, O. "Modelling of the Age Hardening Behaviour of Al–Mg–Si Alloys." *Acta Materialia* 49.1 (2001): 65-75.

[24] Jacobs, M. H. "The Structure of the Metastable Precipitates Formed during Ageing of an Al-Mg-Si Alloy." *Philosophical Magazine* 26.1 (1972): 1-13.

[25] Chakrabarti, D.j, and David E. Laughlin. "Phase Relations and Precipitation in Al–Mg–Si Alloys with Cu Additions." *Progress in Materials Science* 49.3-4 (2004): 389-410.

[26] Chakraborti, N., and H.l. Lukas. "Thermodynamic Optimization of the Mg-Al-Si Phase Diagram." *Calphad* 16.1 (1992): 79-86.

[27] Edwards, G.a., K. Stiller, G.l. Dunlop, and M.j. Couper. "The Precipitation Sequence in Al–Mg–Si Alloys." *Acta Materialia* 46.11 (1998): 3893-904.

[28] Feufel, Harald, T. Gödecke, H. L.Lukas, and F. Sommer. "Investigation of the Al-Mg-Si System by Experiments and Thermodynamic Calculations." *Journal of Alloys and Compounds* 247.1-2 (1997): 31-42.

[29] Lynch, J.p., L.m. Brown, and M.h. Jacobs. "Microanalysis of Age-hardening Precipitates in Aluminium Alloys." *Acta Metallurgica* 30.7 (1982): 1389-395.

[30] Rana, R.S., Rajesh Purhoit, and S. Das. "Reviews on the Influences of Alloying Elements on the Microstructure and Mechanical Properties of Aluminum Alloys and Aluminum Alloy Composites." *International Journal of Scientific and Research Publications* 2.6 (2012): 1-7.

[31] Remøe, M. S. *The Effect of Alloying Elements on the Ductility of Al-Mg-Si*. Thesis. Norwegian University of Science and Technology, 2014

[32] Ceresara, S., E. Di Russo, P. Fiorini, and A. Giarda. "Effect of Si Excess on the Ageing Behaviour of Al□Mg2Si 0.8% Alloy." *Materials Science and Engineering* 5.4 (1970): 220-27.

[33] Zhong, Hao, Paul A. Rometsch, L. Cao, and Y. Estrin. "The Influence of Mg/Si Ratio and Cu Content on the Stretch Formability of 6xxx Aluminium Alloys." *Materials Science and Engineering: A* 651 (2016): 688-97.

[34] ASTM A255 - 10(2014) Standard Test Methods for Determining Hardenability of Steel." *ASTM A255 - 10(2014) Standard Test Methods for Determining Hardenability of Steel*. 2014.

[35] Newkirk, J.w., and D.s. Mackenzie. "The Jominy End Quench for Light-Weight Alloy Development." *Journal of Materials Engineering and Performance* 9.4 (2000): 408-15.

[36] Rometsch, P.a, M.j Starink, and P.j Gregson. "Improvements in Quench Factor Modelling." *Materials Science and Engineering: A* 339.1-2 (2003): 255-64.

[37] Teirlinck, D., F. Zok, J.d. Embury, and M.f. Ashby. "Fracture Mechanism Maps in Stress Space." *Acta Metallurgica* 36.5 (1988): 1213-228.

[38] J.S. Kirkaldy, "Quantitative Prediction of Transformation Hardening in Steels", *Heat Treating*, Vol 4, *ASM Handbook*, ASM International, 1991, p 20–32.

[39] Çengel, Yunus A., and Afshin J. Ghajar. *Heat and Mass Transfer: Fundamentals & Applications*. New York, NY: McGraw-Hill, 2015.

[40] Strobel, Katharina, Mark A. Easton, Lisa Sweet, Malcolm J. Couper, and Jian-Feng Nie. "Relating Quench Sensitivity to Microstructure in 6000 Series Aluminium Alloys." *Materials Transactions* 52.5 (2011): 914-19.

[41] Elmaryami, Abdlmanam S. A., and B. Omar. "Developing 1-Dimensional Transient Heat Transfer Axi-Symmetric MM to Predict the Hardness, Determination LHP and to Study the Effect of Radius on E-LHP of Industrial Quenched Steel Bar." *Heat Transfer Phenomena and Applications* (2012).

[42] Wells, M. A., D. Li, and S. L. Cockcroft. "Influence of Surface Morphology, Water Flow Rate, and Sample Thermal History on the Boiling-water Heat Transfer during Direct-chill Casting of Commercial Aluminum Alloys." *Metall and Materi Trans B Metallurgical and Materials Transactions B* 32.5 (2001): 929-39.

Appendix A

Jominy quenched end test individual hardness profiles:

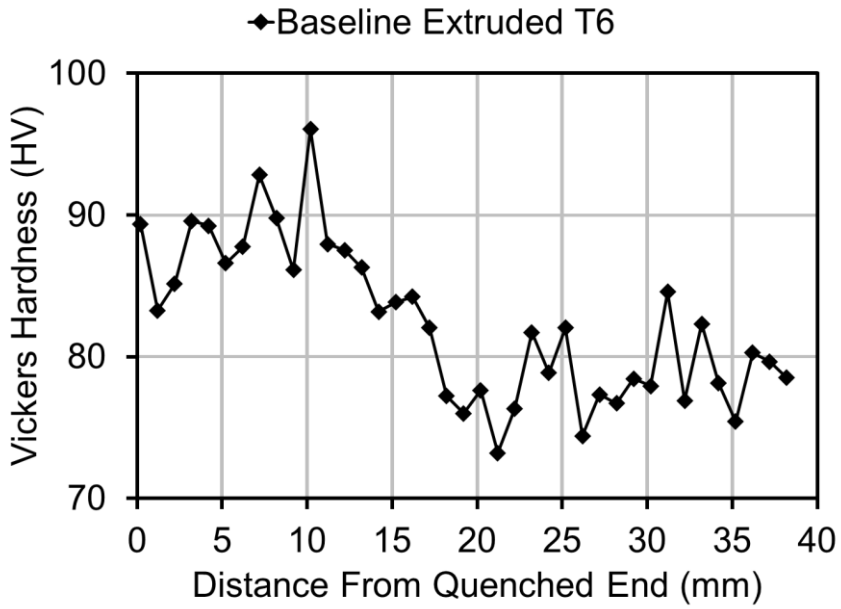

A- 1: Hardness profile of Baseline AA6063 in the T6 condition

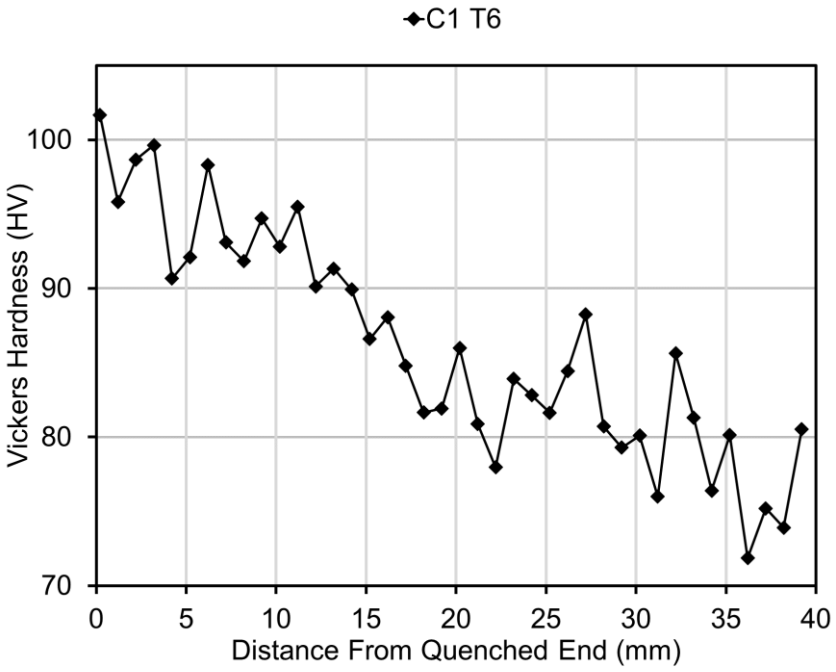

A- 2: Hardness profile of C1 in the T6 condition

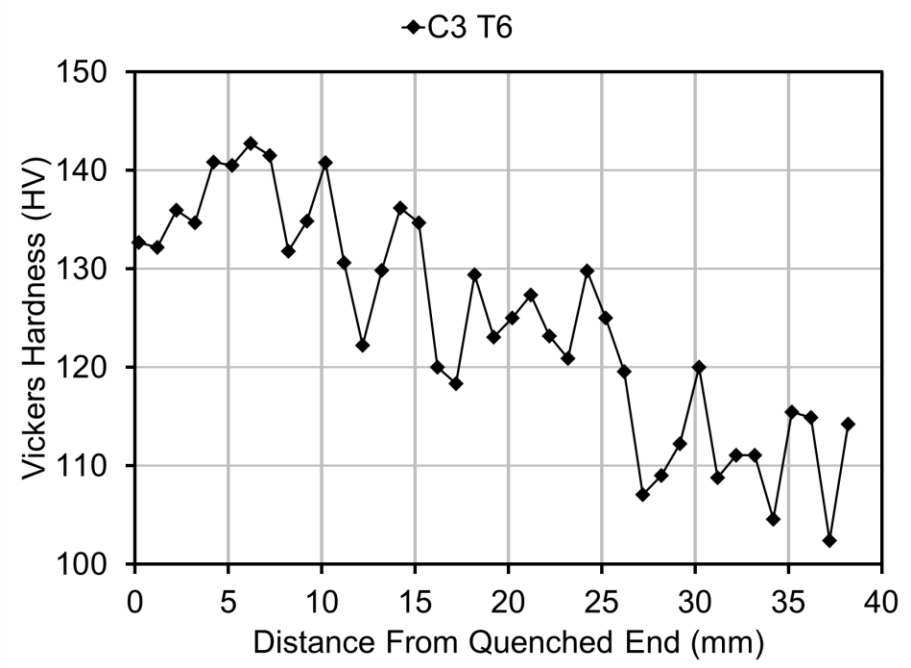

A-3: Hardness profile of C3 in the T6 condition

Tensile test results and extra data:

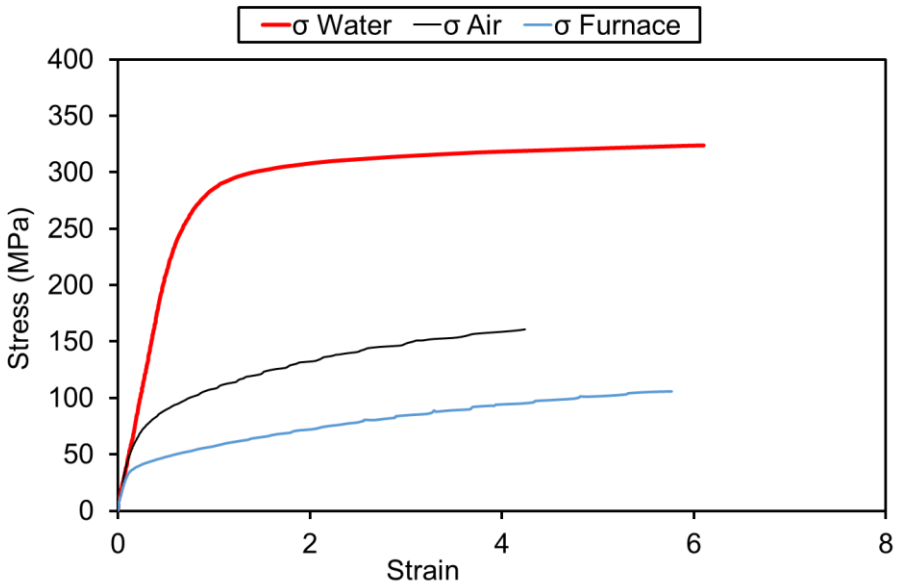

A-4: Yield stress portion of stress-strain curve for C3 alloy in the T6 condition

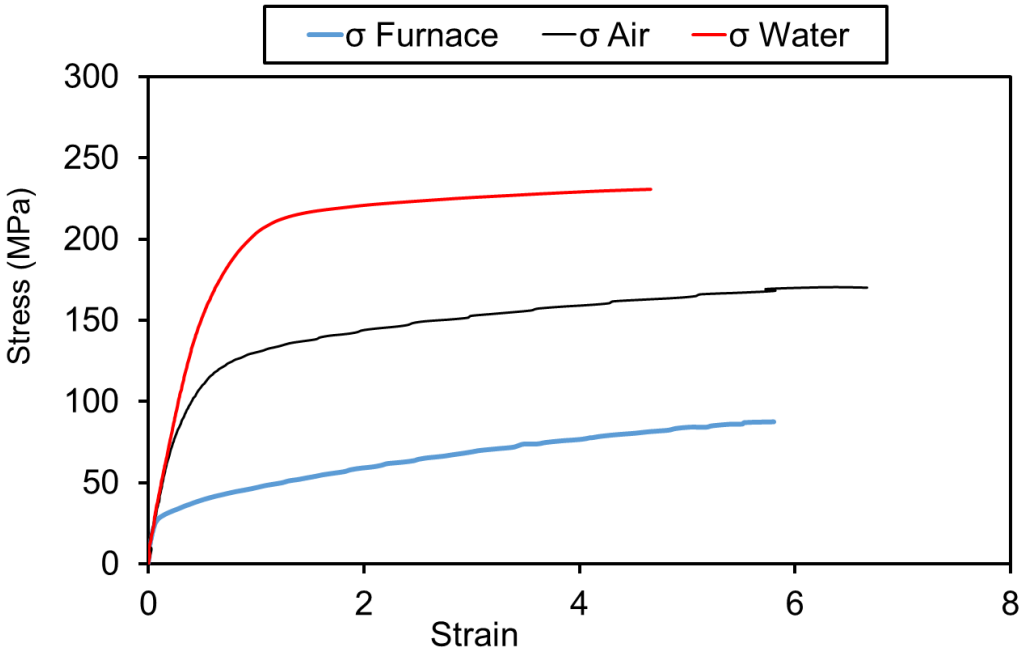

A-5: Yield stress portion of stress-strain curve for C1 alloy in the T6 condition

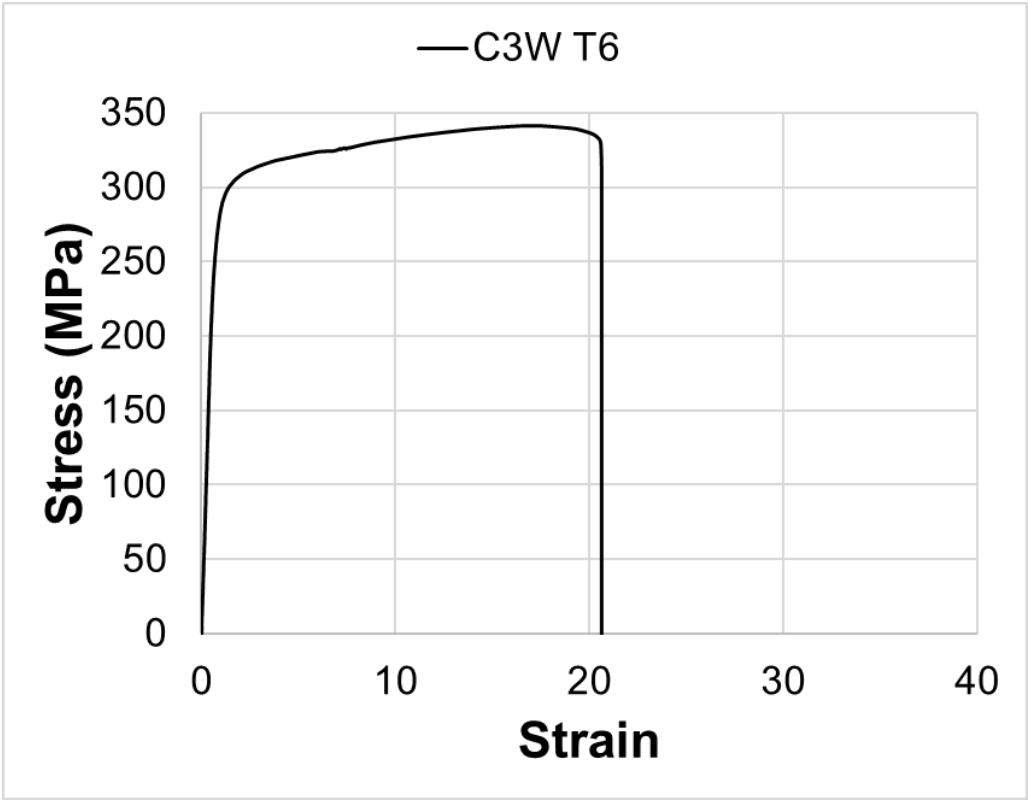

A-6: Stress-strain curve of composition 3 in the water quenched and T6 condition

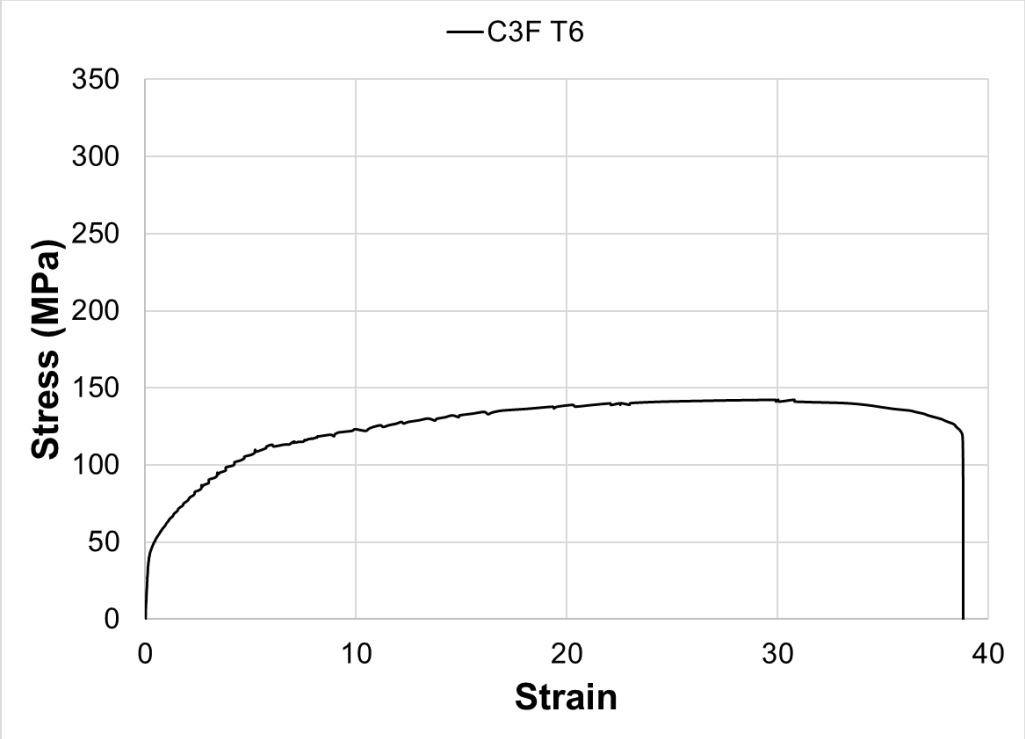

A-7: Stress-strain curve of composition 3 in the furnace cooled and T6 condition

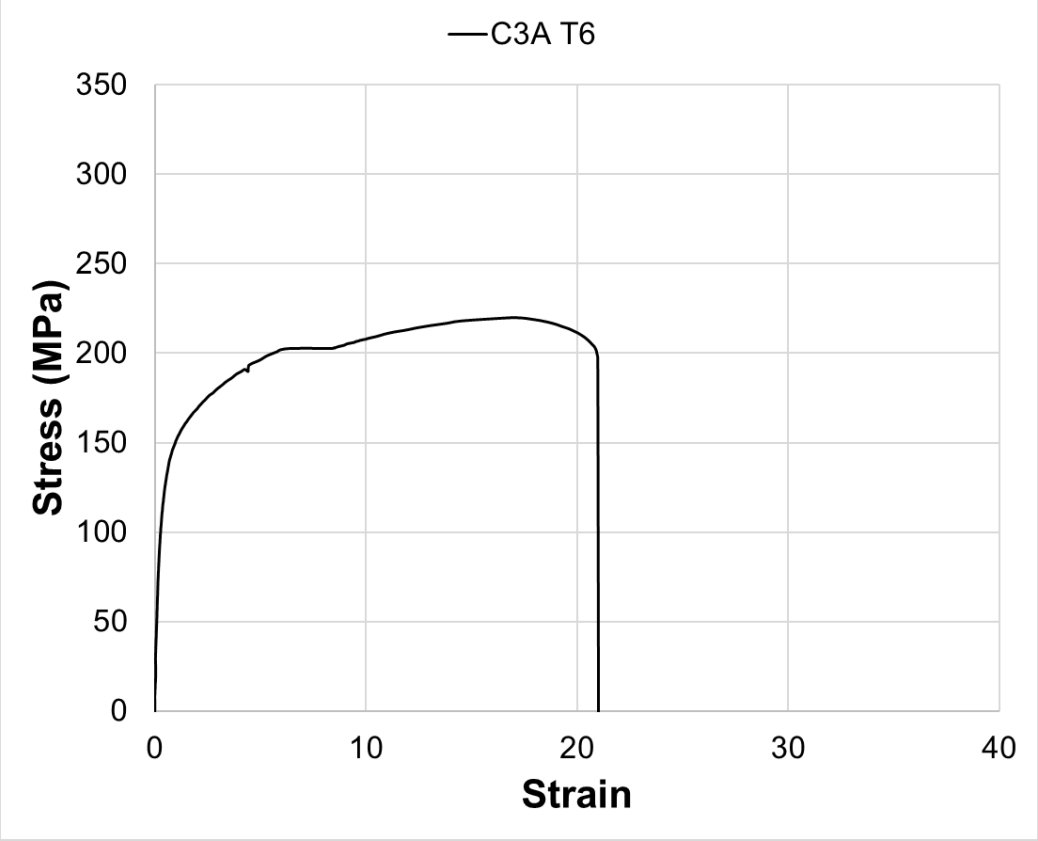

A-8: Stress-strain curve of composition 3 in the air cooled and T6 condition

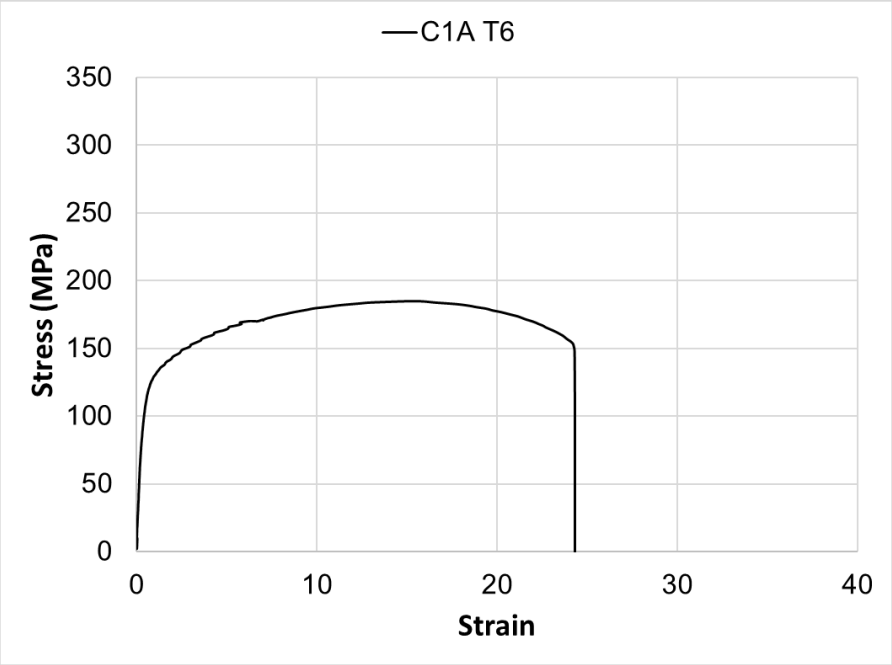

A-9: Stress-strain curve of composition 1 in the air cooled and T6 condition

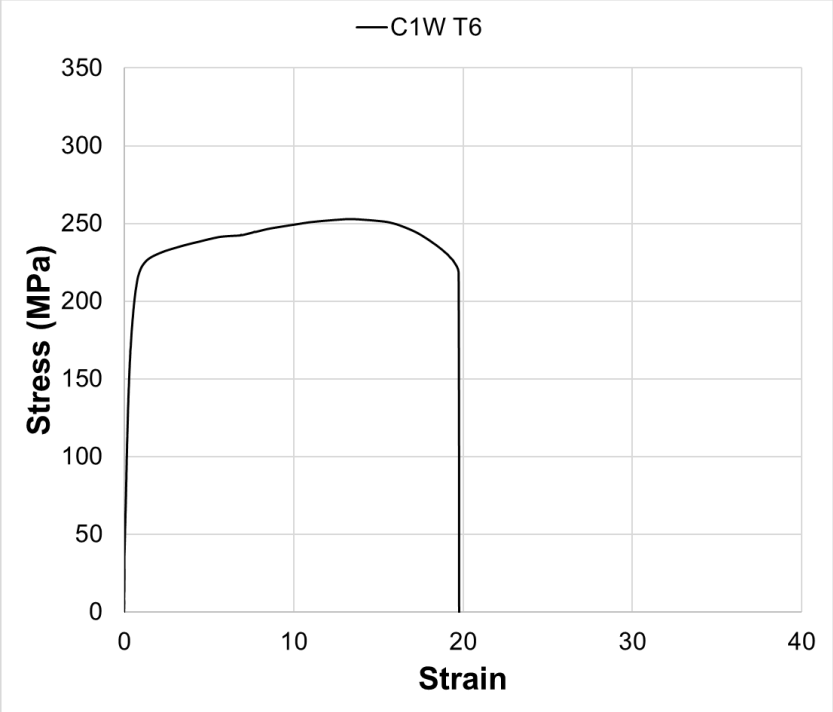

A-10: Stress-strain curve of composition 1 in the water quenched and T6 condition

Time-temperature profiles from extreme cooling rates test:

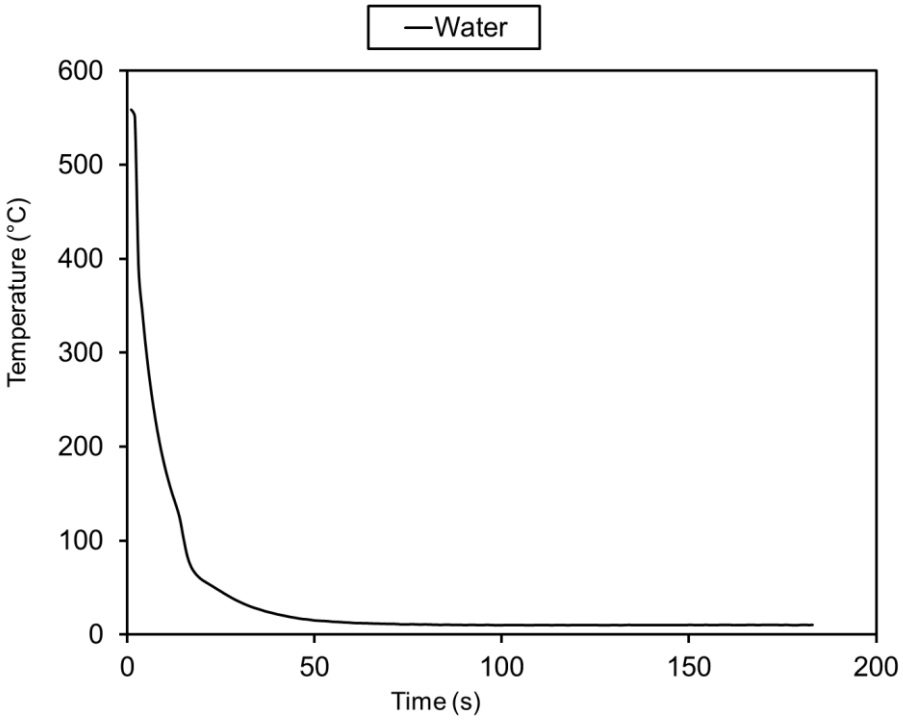

A-11: Time-temperature profile for water quenched AA6063, C1, and C3 alloys

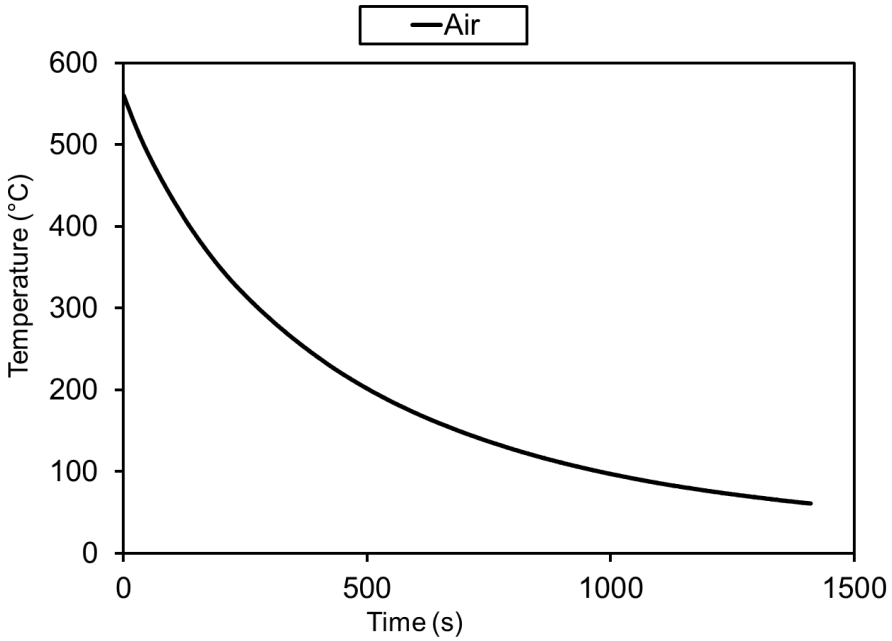

A-12: Time-temperature profile for air cooled AA6063, C1, and C3 alloys

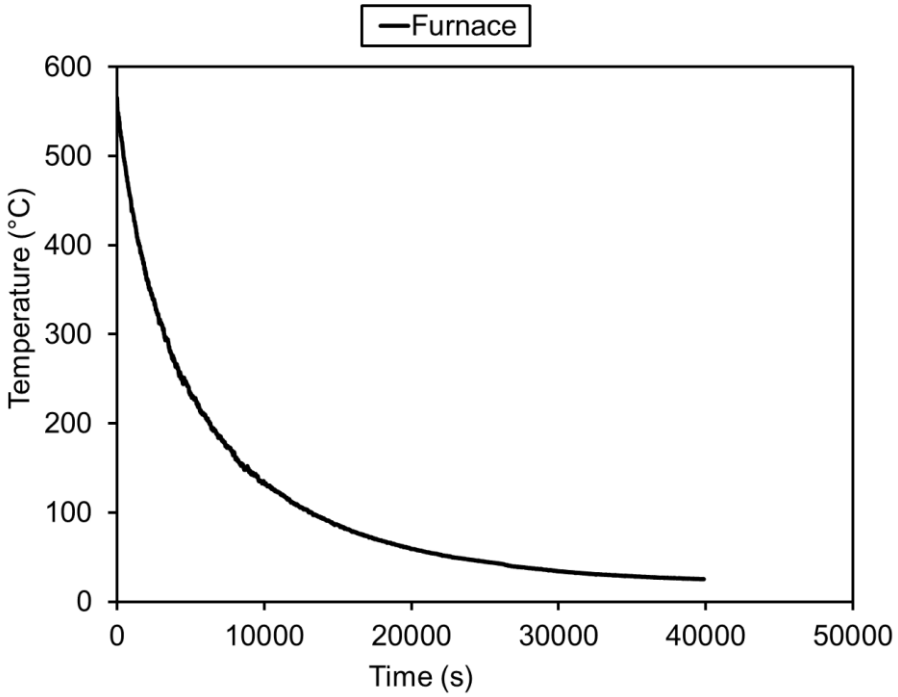

A-13: Time-temperature profile for furnace cooled AA6063, C1, and C3 alloys